

Unsteady motion of a slightly rarefied gas caused by a plate oscillating in its normal direction

Kazuo Aoki

*Mathematics Division, National Center for Theoretical Sciences,
National Taiwan University, Taipei 10617, Taiwan
and Department of Mathematics, National Cheng Kung University, Tainan 70101, Taiwan*

Shingo Kosuge

*Center for Global Leadership Engineering Education, Graduate School of Engineering,
Kyoto University, Kyoto 615-8540, Japan*

Taiga Fujiwara

*Department of Mechanical Engineering and Science, Graduate School of Engineering,
Kyoto University, Kyoto 615-8540, Japan*

Thierry Goudon

Université Côte d'Azur, Inria, CNRS, LJAD, Parc Valrose, 06108 Nice, France

(Received 29 September 2016; published 24 January 2017)

Unsteady motion of a rarefied gas between two parallel plates caused when one of the plates starts a harmonic oscillation in its normal direction is investigated under a slightly rarefied condition, i.e., for small Knudsen numbers. The compressible Navier-Stokes equations are employed and their appropriate temperature jump condition is derived systematically. The equations with the correct boundary conditions are solved numerically to give the unsteady flow field. In particular, the time-periodic solution established at later times is investigated in detail and it is shown that the one-period average of the oscillating part of the momentum and that of the energy transferred from the oscillating plate to the resting one take nonzero values in contrast to the linear theory. This confirms the numerical result based on the Bhatnagar-Gross-Krook model of the Boltzmann equation for intermediate Knudsen numbers [T. Tsuji and K. Aoki, *Microfluid. Nanofluid.* **16**, 1033 (2014)]. It is also shown that the gas approaches the time-periodic motion exponentially fast in time.

DOI: [10.1103/PhysRevFluids.2.013402](https://doi.org/10.1103/PhysRevFluids.2.013402)

I. INTRODUCTION

Moving boundary problems for the Boltzmann and related kinetic equations have attracted much attention in microfluid dynamics and in rarefied gas dynamics (e.g., [1–7]) in connection with the importance of the gas motion caused by an oscillator in microelectromechanical systems (e.g., [8–12]) and of the wave propagation in a rarefied gas (e.g., [13–21]). When a system containing an oscillating boundary is of microscale or in vacuum facilities, the mean free path of the gas molecules can be comparable to the size of the system. In this case, the ordinary continuum gas dynamics is not applicable and is to be replaced by kinetic theory [22–25]. In addition, even when the system is of ordinary size in an atmospheric pressure, if the oscillator makes an oscillation with a very high frequency comparable to the collision frequency of the gas molecules, the ordinary gas dynamics should be replaced by kinetic theory.

In the present paper we consider a fundamental problem containing an oscillating boundary. More specifically, we consider the time-dependent motion of a gas between two infinitely wide plates parallel to each other when one of the plates starts a harmonic oscillation in its normal direction.

This problem, as well as the problem without the stationary plate (i.e., the gas occupies the half space bounded by the oscillating plate), is one of the most fundamental time-dependent problems

in kinetic theory and has been investigated by many authors (see, e.g., [13–21]). However, many of the existing works are based on the linearized setting, in which the speed of the oscillating plate is much smaller than the sonic speed, and consider the time-periodic state. In the present study, we focus our attention on the fully nonlinear setting in which the speed and amplitude of the oscillation of the plate can be large, as studied in [15,16,20,21].

The present problem was investigated numerically in a recent paper [21] on the basis of the Bhatnagar-Gross-Krook (BGK) model of the Boltzmann equation [26,27] and the transient behavior of the gas approaching a time-periodic state was clarified. In this problem, the oscillating plate creates and propagates discontinuities in the velocity distribution function of the gas molecules continuously. In [21], a numerical method that can describe the propagation of the discontinuities proposed in [4] was used and an accurate numerical solution was obtained for a wide range of the Knudsen number, the ratio of the mean free path of the gas molecules to the characteristic length of the system. However, since the method is computationally expensive, it is hard to obtain the long-time behavior as well as the solution for small Knudsen numbers.

For small Knudsen numbers, however, it is commonly known that the Navier-Stokes equations can describe the behavior of the gas well if appropriate slip boundary conditions are used. This may give a good alternative to the Boltzmann and its model equations that enables us to investigate the long-time behavior more easily. In fact, the slip flow theory has been established by Sone in a series of papers by a systematic asymptotic analysis for the Boltzmann equation [28–33] (see also [24,25]). For ordinary solid boundaries, the theory consists of (see [24,25]) the linear theory for small Reynolds numbers [28,29,31], the weakly nonlinear theory for finite Reynolds numbers [29–31], the partially nonlinear theory for finite Reynolds numbers [32], and the fully nonlinear theory for large Reynolds numbers [33], each of which provides appropriate fluid-dynamic equations, slip boundary conditions, and the corrections in the vicinity of the boundary (Knudsen layer). However, the theory is restricted to time-independent problems, so it cannot be applied to the present problem. The linear theory has been extended to time-dependent problems recently [34–36] (see also Sec. 3.7 in [25]). However, since the boundary is assumed not to be moving in its normal direction, it is not applicable to the present problem even if we consider the linear setting.

For this reason, we need a different framework for the present problem. In the present study, we have decided to use the compressible Navier-Stokes equations as our basic equation. However, if we search the appropriate and correct slip boundary conditions for the compressible Navier-Stokes equations that can be applied immediately to the present problem with a moving plate, we notice that it is hard to find them in the literature. For this reason, following the standard procedure [24,25,37,38], that is, the analysis of the Knudsen layer combined with the Chapman-Enskog expansion, we try to derive the slip boundary conditions, specialized to the present problem, in a systematic way. Then we apply the compressible Navier-Stokes equations and the derived slip conditions, consisting of the no-slip condition for the flow velocity and a jump condition for the temperature, to the present problem and investigate the unsteady behavior of the gas and the process of approach to a time-periodic state numerically.

The paper is organized as follows. After the introduction in Sec. I, we state the problem and the assumptions in Sec. II and formulate the problem using kinetic theory in Sec. III. Then we summarize the Chapman-Enskog solution and the compressible Navier-Stokes equations in Sec. IV and the jump boundary conditions in Sec. V. Section VI is devoted to the explanation of the numerical method for the compressible Navier-Stokes equations, and the numerical results are given in Sec. VII. Section VIII contains short concluding remarks. In addition, we summarize the basic matters concerning the collision operator of the Boltzmann equation in Appendix A, derive the slip boundary conditions in Appendix B, and discuss the accuracy of the numerical solution in Appendix C.

II. PROBLEM AND ASSUMPTIONS

Let us consider a gas between two infinitely wide plates, kept at temperature \tilde{T}_0 and parallel to each other. One of the plates is located at $\tilde{x}_1 = \tilde{a}_w$ (greater than 0) and the other at $\tilde{x}_1 = \tilde{d}$ (greater

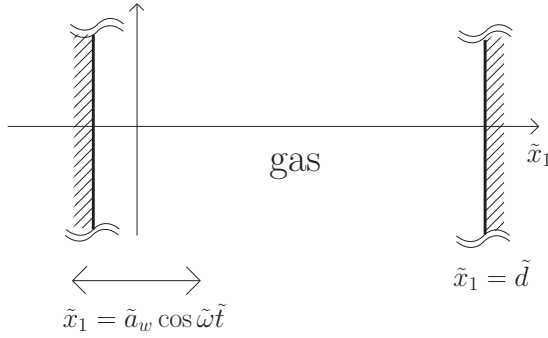


FIG. 1. Gas between an oscillating plate and a stationary plate.

than \tilde{a}_w), where $(\tilde{x}_1, \tilde{x}_2, \tilde{x}_3)$ is the Cartesian coordinate system, and the gas is in a uniform equilibrium state at rest at density $\tilde{\rho}_0$ and temperature \tilde{T}_0 . At time $\tilde{t} = 0$, the plate at $\tilde{x}_1 = \tilde{a}_w$ starts a harmonic oscillation with amplitude \tilde{a}_w and angular frequency $\tilde{\omega}$ around $\tilde{x}_1 = 0$, that is, the location of the plate is described as $\tilde{x}_1 = \tilde{x}_w(\tilde{t})$, with $\tilde{x}_w(\tilde{t}) = \tilde{a}_w \cos \tilde{\omega} \tilde{t}$ for $\tilde{t} \geq 0$ (see Fig. 1). We investigate the unsteady motion of the gas numerically under the following assumptions.

- (i) The behavior of the gas is described by the Boltzmann equation.
- (ii) The gas molecules undergo diffuse reflection on the surfaces of the plates.
- (iii) The problem is spatially one dimensional, so the physical quantities depend on neither \tilde{x}_2 nor \tilde{x}_3 , and the macroscopic gas flow is perpendicular to the plates.
- (iv) The mean free path of the gas molecules is much shorter than the characteristic length of the system. That is, the gas is slightly rarefied.

Because of assumption (iv), we will analyze the problem using the Navier-Stokes equations and the appropriate jump conditions on the plates that are consistent with the assumptions (i) and (ii).

III. FORMULATION OF THE PROBLEM USING KINETIC THEORY

A. Notation

Before formulating the problem, we introduce some notation. Let $\tilde{\zeta}_i$ be the velocity of gas molecules, $\tilde{f}(\tilde{t}, \tilde{x}_1, \tilde{\zeta}_i)$ the velocity distribution function of gas molecules, $\tilde{\rho}(\tilde{t}, \tilde{x}_1)$ the mass density of the gas, $\tilde{v}_i(\tilde{t}, \tilde{x}_1) = (\tilde{v}_1(\tilde{t}, \tilde{x}_1), 0, 0)$ the flow velocity of the gas [cf. assumption (iii)], $\tilde{T}(\tilde{t}, \tilde{x}_1)$ the temperature of the gas, and $\tilde{p}(\tilde{t}, \tilde{x}_1) = R\tilde{\rho}\tilde{T}$ the pressure of the gas, where R is the gas constant per unit mass ($R = k_B/m$ with the Boltzmann constant k_B and the mass of a gas molecule m). In addition, let $\tilde{p}_{ij}(\tilde{t}, \tilde{x}_1)$ be the stress tensor and $\tilde{q}_i(\tilde{t}, \tilde{x}_1)$ the heat-flow vector. We set the reference time \tilde{t}_0 , the reference speed \tilde{c}_0 , and the reference length L as

$$\tilde{t}_0 = 1/\tilde{\omega}, \quad \tilde{c}_0 = (2R\tilde{T}_0)^{1/2}, \quad L = \tilde{c}_0\tilde{t}_0 = (2R\tilde{T}_0)^{1/2}/\tilde{\omega}. \quad (1)$$

Then we introduce the dimensionless quantities $(t, x_i, \zeta_i, f, \rho, v_i, T, p, p_{ij}, q_i)$ that correspond to $(\tilde{t}, \tilde{x}_i, \tilde{\zeta}_i, \tilde{f}, \tilde{\rho}, \tilde{v}_i, \tilde{T}, \tilde{p}, \tilde{p}_{ij}, \tilde{q}_i)$ by the relations

$$\begin{aligned} t &= \tilde{t}/\tilde{t}_0 = \tilde{t}\tilde{\omega}, & x_i &= \tilde{x}_i/L, & \zeta_i &= \tilde{\zeta}_i/\tilde{c}_0, \\ f(t, x_1, \zeta_i) &= (\tilde{c}_0^3/\tilde{\rho}_0)\tilde{f}(\tilde{t}, \tilde{x}_1, \tilde{\zeta}_i), \\ \rho(t, x_1) &= \tilde{\rho}/\tilde{\rho}_0, & v_i(t, x_1) &= (\tilde{v}_i(t, x_1), 0, 0) = \tilde{v}_i/\tilde{c}_0, \\ T(t, x_1) &= \tilde{T}/\tilde{T}_0, & p(t, x_1) &= \tilde{p}/\tilde{p}_0, \\ p_{ij}(t, x_1) &= \tilde{p}_{ij}/\tilde{p}_0, & q_i(t, x_1) &= \tilde{q}_i/\tilde{p}_0\tilde{c}_0, \end{aligned} \quad (2)$$

where $\tilde{p}_0 = R\tilde{\rho}_0\tilde{T}_0$ is the reference pressure based on $\tilde{\rho}_0$ and \tilde{T}_0 . Then the dimensionless macroscopic quantities ρ , v_i , T , p , p_{ij} , and q_i are expressed as follows [25]:

$$\rho = \int f d\boldsymbol{\zeta}, \quad v_i = \frac{1}{\rho} \int \zeta_i f d\boldsymbol{\zeta}, \quad T = \frac{2}{3\rho} \int (\zeta_i - v_i)^2 f d\boldsymbol{\zeta}, \quad p = \rho T, \quad (3a)$$

$$p_{ij} = 2 \int (\zeta_i - v_i)(\zeta_j - v_j) f d\boldsymbol{\zeta}, \quad q_i = \int (\zeta_i - v_i)(\zeta_j - v_j)^2 f d\boldsymbol{\zeta}, \quad (3b)$$

where $d\boldsymbol{\zeta} = d\zeta_1 d\zeta_2 d\zeta_3$. Here and in what follows, the summation convention (i.e., $a_i b_i = a_1 b_1 + a_2 b_2 + a_3 b_3$ and $a_i^2 = a_1^2 + a_2^2 + a_3^2$) is used and the domain of integration with respect to ζ_i is its whole space unless otherwise stated. The assumption $v_2 = v_3 = 0$ [assumption (iii)] means that we implicitly assume that f is cylindrically symmetric in ζ_i , i.e., $f = f(t, x_1, \zeta_1, \sqrt{\zeta_2^2 + \zeta_3^2})$. Therefore, some components of p_{ij} and q_i vanish, that is,

$$p_{12} = p_{21} = p_{23} = p_{32} = p_{31} = p_{13} = 0, \quad q_2 = q_3 = 0. \quad (4)$$

Let us denote by \tilde{v}_w the velocity (in the \tilde{x}_1 direction) of the oscillating plate, i.e., $\tilde{v}_w = -\tilde{a}_w \tilde{\omega} \sin \tilde{\omega} \tilde{t}$. We introduce the dimensionless position $x_w(t)$ and velocity $v_w(t)$ of the oscillating plate and the dimensionless parameters a_w and d corresponding to the amplitude \tilde{a}_w of the oscillating plate and the position \tilde{d} of the resting plate by

$$x_w(t) = \tilde{x}_w/L, \quad v_w(t) = \tilde{v}_w/\tilde{c}_0, \quad a_w = \tilde{a}_w/L, \quad d = \tilde{d}/L. \quad (5)$$

Then

$$x_w(t) = a_w \cos t, \quad v_w(t) = -a_w \sin t. \quad (6)$$

It should be noted that the dimensionless amplitude (and speed) of the plate a_w is of the order of the Mach number Ma based on the maximum speed of the plate, that is,

$$a_w = \sqrt{5/6} \text{Ma}, \quad \text{Ma} = \tilde{a}_w \tilde{\omega} / [(5/3)R\tilde{T}_0]^{1/2}. \quad (7)$$

B. Basic equations

The dimensionless Boltzmann equation [25] in the present spatially-one-dimensional problem is written as

$$\frac{\partial f}{\partial t} + \zeta_1 \frac{\partial f}{\partial x_1} = \frac{1}{\epsilon} J(f, f), \quad (8)$$

with a small parameter ϵ ,

$$\epsilon = (\sqrt{\pi}/2) \text{Kn} = (\sqrt{\pi}/2)(l_0/L), \quad (9)$$

where Kn is the Knudsen number and l_0 is the mean free path of the gas molecules at the initial equilibrium state at rest. In Eq. (8), $J(f, f)$ is the dimensionless collision term, the explicit form of which is given in Appendix A.

The diffuse-reflection condition [25] on the moving boundary is written as

$$f(t, x_w(t), \zeta_i) = \frac{\sigma_w}{\pi^{3/2}} \exp\left(-\{[\zeta_1 - v_w(t)]^2 + \zeta_2^2 + \zeta_3^2\}\right) \quad \text{for } \zeta_1 - v_w(t) > 0, \quad (10a)$$

$$\sigma_w = -2\pi^{1/2} \int_{\zeta_1 - v_w(t) < 0} [\zeta_1 - v_w(t)] f(t, x_w(t), \zeta_i) d\boldsymbol{\zeta}, \quad (10b)$$

where x_w and v_w are given by Eq. (6), and that on the plate at rest is

$$f(t, d, \zeta_i) = \frac{\sigma_w}{\pi^{3/2}} \exp[-(\zeta_1^2 + \zeta_2^2 + \zeta_3^2)] \quad \text{for } \zeta_1 < 0, \quad (11a)$$

$$\sigma_w = 2\pi^{1/2} \int_{\zeta_1 > 0} \zeta_1 f(t, d, \zeta_i) d\zeta. \quad (11b)$$

The initial condition is

$$f(0, x_1, \zeta_i) = \pi^{-3/2} \exp[-(\zeta_1^2 + \zeta_2^2 + \zeta_3^2)] \quad \text{for } a_w \leq x_1 \leq d. \quad (12)$$

It is seen from Eqs. (8), (10a), (11a), and (12) that the problem is characterized by the three parameters ϵ , a_w , and d .

IV. CHAPMAN-ENSKOG SOLUTION AND THE COMPRESSIBLE NAVIER-STOKES EQUATIONS

The Chapman-Enskog expansion [25,39,40] is a well-known procedure to derive the Euler and Navier-Stokes equations for a compressible fluid from the Boltzmann equation. In this section we summarize the Chapman-Enskog solution obtained by the Chapman-Enskog expansion and the resulting compressible Navier-Stokes equations for the present spatially-one-dimensional problem. We basically follow the description and notation of Sec. B4 in [25], but note that some symbols are not exactly the same. For example, the caret indicating the dimensionless quantities in [25] is omitted here and \mathcal{C}_i in [25] is denoted by C_i here.

The first-order Chapman-Enskog solution for the spatially-one-dimensional Boltzmann equation (8) can be expressed as

$$f = f_{\text{CE}}^{(1)} + O(\epsilon^2) = f^{(0)} + f^{(1)}\epsilon + O(\epsilon^2). \quad (13)$$

Here the leading-order term $f^{(0)}$ is a local Maxwellian distribution

$$f^{(0)} = \frac{\rho}{(\pi T)^{3/2}} \exp\left(-\frac{(\zeta_1 - v_1)^2 + \zeta_2^2 + \zeta_3^2}{T}\right) = \frac{\rho}{T^{3/2}} E(C) \quad (14)$$

and the first-order term $f^{(1)}$ takes the form

$$f^{(1)} = f^{(0)}\Psi, \quad (15a)$$

$$\Psi = -\frac{1}{\rho T^{1/2}} \left(C_1^2 - \frac{1}{3} C^2 \right) \frac{\partial v_1}{\partial x_1} \mathcal{B}^{(0)}(C, T) - \frac{1}{\rho T} C_1 \frac{\partial T}{\partial x_1} \mathcal{A}(C, T), \quad (15b)$$

where

$$C_1 = \frac{\zeta_1 - v_1}{T^{1/2}}, \quad C_2 = \frac{\zeta_2}{T^{1/2}}, \quad C_3 = \frac{\zeta_3}{T^{1/2}}, \quad (16a)$$

$$E(C) = \pi^{-3/2} \exp(-C^2), \quad C = (C_1^2 + C_2^2 + C_3^2)^{1/2}, \quad (16b)$$

and $\mathcal{B}^{(0)}(C, T)$ and $\mathcal{A}(C, T)$ are, in principle, known functions of C and T , which are specified in Appendix A.

The expansion (13) is designed in such a way that ρ , v_1 , and T in Eq. (14) are, respectively, the density, the x_1 component of the flow velocity, and the temperature associated with f [cf. Eq. (3a)]. Therefore, we construct the remainder so that, at any order, the corresponding moments vanish,

that is,

$$\int (1, \zeta_1, \zeta_i^2) f^{(1)} d\zeta = 0, \quad \int (1, \zeta_1, \zeta_i^2) O(\epsilon^2) d\zeta = 0. \quad (17)$$

Formulas (15) that define $f^{(1)}$ fulfill this requirement.

With Eq. (13), p_{ij} and q_i in Eq. (3b) become

$$p_{11} = p - \frac{4}{3}\epsilon\Gamma_1(T)\frac{\partial v_1}{\partial x_1}, \quad p_{22} = p_{33} = p, \quad p_{ij} = 0 \quad (i \neq j), \quad (18a)$$

$$q_1 = -\frac{5}{4}\epsilon\Gamma_2(T)\frac{\partial T}{\partial x_1}, \quad q_2 = q_3 = 0, \quad (18b)$$

where $\Gamma_1(T)$ and $\Gamma_2(T)$ are expressed as

$$\Gamma_1(T) = \frac{8}{15\sqrt{\pi}}T^{1/2} \int_0^\infty C^6 \mathcal{B}^{(0)}(C, T) e^{-C^2} dC, \quad (19a)$$

$$\Gamma_2(T) = \frac{16}{15\sqrt{\pi}}T^{1/2} \int_0^\infty C^6 \mathcal{A}(C, T) e^{-C^2} dC \quad (19b)$$

and are related to the viscosity μ and the thermal conductivity λ as

$$\mu = (\tilde{p}_0 L / \tilde{c}_0) \epsilon \Gamma_1(T) = (\sqrt{\pi}/2)(\tilde{p}_0 l_0 / \tilde{c}_0) \Gamma_1(T), \quad (20a)$$

$$\lambda = (5/4)(\tilde{p}_0 \tilde{c}_0 L / \tilde{T}_0) \epsilon \Gamma_2(T) = (5\sqrt{\pi}/8)(\tilde{p}_0 \tilde{c}_0 l_0 / \tilde{T}_0) \Gamma_2(T). \quad (20b)$$

For hard-sphere molecules and the BGK model, $\Gamma_1(T)$ and $\Gamma_2(T)$ are explicitly expressed as, respectively,

$$\Gamma_1(T) = 1.270\,042\,427T^{1/2}, \quad \Gamma_2(T) = 1.922\,284\,066T^{1/2}, \quad (21a)$$

$$\Gamma_1(T) = \Gamma_2(T) = T. \quad (21b)$$

With Eq. (18), the Maxwell transport equations, which are derived by integrating Eq. (8) times $(1, \zeta_i, \zeta_j^2)$ over the whole space of ζ_i , reduce to the compressible Navier-Stokes equations

$$\frac{\partial \rho}{\partial t} + \frac{\partial(\rho v_1)}{\partial x_1} = 0, \quad (22a)$$

$$\frac{\partial(\rho v_1)}{\partial t} + \frac{\partial(\rho v_1^2)}{\partial x_1} = -\frac{1}{2} \frac{\partial p}{\partial x_1} + \frac{2}{3} \epsilon \frac{\partial}{\partial x_1} \left[\Gamma_1(T) \frac{\partial v_1}{\partial x_1} \right], \quad (22b)$$

$$\frac{\partial}{\partial t} \left[\rho \left(\frac{3}{2} T + v_1^2 \right) \right] + \frac{\partial}{\partial x_1} \left[\rho v_1 \left(\frac{5}{2} T + v_1^2 \right) \right] = \frac{5}{4} \epsilon \frac{\partial}{\partial x_1} \left[\Gamma_2(T) \frac{\partial T}{\partial x_1} \right] + \frac{4}{3} \epsilon \frac{\partial}{\partial x_1} \left[\Gamma_1(T) \frac{\partial v_1}{\partial x_1} v_1 \right], \quad (22c)$$

where $p = \rho T$ [Eq. (3a)], and the x_2 and x_3 components of the momentum equation become trivial (i.e., $0 = 0$). If we substitute Eq. (13) with ρ , v_1 , and T satisfying the Navier-Stokes equations (22) into the Boltzmann equation (8) multiplied by ϵ , then we observe that the expansion (13) satisfies the latter with the error of $O(\epsilon^2)$.

V. JUMP BOUNDARY CONDITIONS

In the first-order Chapman-Enskog solution (13), which corresponds to the Navier-Stokes equations (22), the boundary conditions on the plates (10a) and (11a) are not taken into account. To be consistent with the fact that the term up to $O(\epsilon)$ is considered in Eq. (13), we need to satisfy the boundary conditions up to the order of ϵ .

We first try to satisfy the boundary conditions with the Chapman-Enskog solution (13). If we recall that the leading-order term $f^{(0)}$ is a local Maxwellian [Eq. (14)], it can be made to satisfy Eqs. (10a) and (11a) by assuming that

$$v_1 = v_w(t), \quad T = 1 \quad \text{at } x_1 = x_w(t), \quad (23a)$$

$$v_1 = 0, \quad T = 1 \quad \text{at } x_1 = d. \quad (23b)$$

On the other hand, in order that the first-order term $f^{(1)}$ satisfies Eqs. (10a) and (11a) at the order of ϵ , we need to impose the following conditions:

$$\frac{\partial v_1}{\partial x_1} = 0, \quad \frac{\partial T}{\partial x_1} = 0 \quad \text{at } x_1 = x_w(t), d. \quad (24)$$

However, the constraints on the plates [Eqs. (23) and (24)] are too many as the boundary conditions for the Navier-Stokes equations (22). Therefore, this approach does not work. However, the fact that the choice (23) works at the zeroth order in ϵ suggests that

$$v_1 - v_w(t) = O(\epsilon), \quad T - 1 = O(\epsilon) \quad \text{at } x_1 = x_w(t), \quad (25a)$$

$$v_1 = O(\epsilon), \quad T - 1 = O(\epsilon) \quad \text{at } x_1 = d. \quad (25b)$$

In order to obtain the solution satisfying the boundary conditions, it is required to introduce the kinetic boundary layer, the so-called Knudsen layer, with thickness of the order of ϵ adjacent to the plates. To be more specific, we seek the solution in the form

$$f = f_{\text{CE}}^{(1)} + f^{(0)}\Phi\epsilon + O(\epsilon^2) = f^{(0)}(1 + \Psi\epsilon + \Phi\epsilon) + O(\epsilon^2), \quad (26)$$

where we use Eqs. (14) and (15) and Φ is the correction inside the Knudsen layer. We note that Φ has a length scale of variation of the order of ϵ in the direction normal to the boundary and vanishes outside the Knudsen layer. The correction is introduced only at the order of ϵ because, as we saw, the leading-order term $f^{(0)}$ of the Chapman-Enskog expansion could be made to satisfy the boundary conditions.

The analysis of the Knudsen-layer correction Φ determines the boundary conditions for the Navier-Stokes equations (22) that are correct up to the order of ϵ . Leaving the detailed analysis of Φ and the process of deriving the boundary conditions to Appendix B, we summarize the resulting boundary conditions here, that is,

$$v_1 - v_w(t) = 0, \quad T - 1 = \frac{1}{\rho} \frac{\partial v_1}{\partial x_1} \alpha_v \epsilon + \frac{1}{\rho} \frac{\partial T}{\partial x_1} \alpha_T \epsilon \quad \text{at } x_1 = x_w(t), \quad (27a)$$

$$v_1 = 0, \quad T - 1 = \frac{1}{\rho} \frac{\partial v_1}{\partial x_1} \alpha_v \epsilon - \frac{1}{\rho} \frac{\partial T}{\partial x_1} \alpha_T \epsilon \quad \text{at } x_1 = d, \quad (27b)$$

where α_v and α_T are constants that depend on the model for the intermolecular collision. We refer the reader to Appendix B for further explanations of these formulas [see in particular the comments after Eq. (B38), which explain the changes of sign arising in Eqs. (27a) and (27b)]. For hard-sphere molecules and for the BGK model, the coefficients α_v and α_T are given as, respectively,

$$\alpha_v = 0.45957, \quad \alpha_T = 2.4001, \quad (28a)$$

$$\alpha_v = 0.44045, \quad \alpha_T = 1.30272. \quad (28b)$$

These values are for the diffuse reflection condition. For different boundary conditions of ordinary type, these constants take different values, the form of the boundary conditions (27) being unchanged. Although the velocity v_1 is the same as that of the plate, the temperature T differs from that of the plates, that is, there is a *temperature jump* of $O(\epsilon)$. The term containing α_T is the usual temperature jump proportional to the temperature gradient normal to the plates. The term containing α_v is the

jump proportional to the normal stress, which becomes higher order in the steady problems with small Mach number flows. We note that [15] contains the numerical analysis of the present problem using the compressible Navier-Stokes equations with slip boundary conditions. However, the temperature jump condition used there includes neither the term proportional to the normal stress nor the factor $1/\rho$ [cf. Eq. (27)]. In the linearized problem, ρ is replaced by its reference value $\rho = 1$, so the factor $1/\rho$ does not appear. However, in the nonlinear problem, there is a significant density change in the gas and the temperature jump should be proportional to the local Knudsen number, not the global one. Since the local Knudsen number is expressed as ϵ/ρ , the factor $1/\rho$ appears in Eq. (27).

The initial condition for the Navier-Stokes equations corresponding to that for the Boltzmann equation (12) is

$$\rho = 1, \quad v_1 = 0, \quad T = 1 \quad \text{at } t = 0. \quad (29)$$

We are going to solve the Navier-Stokes equations (22) numerically under the boundary conditions (27) and the initial condition (29). In the present problem, the initial condition (12) for the Boltzmann equation is consistent with the first-order Chapman-Enskog solution (13) and satisfies the boundary conditions (10a) and (11a) at $t = 0$. In addition, the left plate starts the motion gradually with the fluid-dynamic time scale. Therefore, the initial layer does not appear. In other words, the Navier-Stokes equations with the initial condition (29) describe the initial stage of the gas motion correctly.

VI. NUMERICAL METHOD

In this section we explain the numerical method used in the computation of Eqs. (22), (27), and (29). For brevity, we omit the subscript 1 of x_1 and v_1 in the present section, i.e., we let

$$x = x_1, \quad v = v_1. \quad (30)$$

A. Numerical scheme

Let us divide the region of the gas $x_w(t) \leq x \leq d$ into N cells by the grid points $x_j(t)$ ($j = 0, \dots, N$) with $x_0(t) = x_w(t)$ and $x_N(t) = d$, which move with time. In the case of uniform cells, $x_j(t) = x_w(t) + (j/N)[d - x_w(t)]$. We call the interval $x_{j-1}(t) \leq x \leq x_j(t)$ the j th cell and define the center of the j th cell $x_{j-1/2}(t)$ as the middle point, i.e., $x_{j-1/2}(t) = [x_{j-1}(t) + x_j(t)]/2$.

We consider the spatially-one-dimensional equation of the form

$$\frac{\partial F}{\partial t} + \frac{\partial G}{\partial x} = 0, \quad (31)$$

where $F(t, x)$ and $G(t, x)$ are functions of x and t . For the Navier-Stokes equations, F and G are given by

$$F = \rho, \quad G = \rho v \quad (32)$$

for Eq. (22a),

$$F = \rho v, \quad G = \rho v^2 + \frac{1}{2}p - \frac{2}{3}\epsilon\Gamma_1(T)\frac{\partial v}{\partial x} \quad (33)$$

for Eq. (22b), and

$$F = \rho v^2 + \frac{3}{2}\rho T, \quad G = \left(\rho v^2 + \frac{5}{2}\rho T\right)v - \frac{5}{4}\epsilon\Gamma_2(T)\frac{\partial T}{\partial x} - \frac{4}{3}\epsilon\Gamma_1(T)v\frac{\partial v}{\partial x} \quad (34)$$

for Eq. (22c). We try to discretize this equation on the system of moving grids $x_i(t)$.

Let us integrate Eq. (31) over the interval $[x_{j-1}(t), x_j(t)]$ in x and then $[t, t + \Delta t]$ in t :

$$\int_t^{t+\Delta t} \int_{x_{j-1}(\tau)}^{x_j(\tau)} \frac{\partial F}{\partial \tau} dx d\tau + \int_t^{t+\Delta t} \int_{x_{j-1}(\tau)}^{x_j(\tau)} \frac{\partial G}{\partial x} dx d\tau = 0. \quad (35)$$

The second term on the left-hand side is transformed as follows:

$$\begin{aligned}
 \int_t^{t+\Delta t} \int_{x_{j-1}(\tau)}^{x_j(\tau)} \frac{\partial G}{\partial x} dx d\tau &= \int_t^{t+\Delta t} [G(\tau, x_j(\tau)) - G(\tau, x_{j-1}(\tau))] d\tau \\
 &\simeq [G(t, x_j(t)) - G(t, x_{j-1}(t))] \Delta t \\
 &\simeq [G(t + \Delta t, x_j(t + \Delta t)) - G(t + \Delta t, x_{j-1}(t + \Delta t))] \Delta t \\
 &\simeq [G(t, x_j(t + \Delta t)) - G(t, x_{j-1}(t + \Delta t))] \Delta t. \tag{36}
 \end{aligned}$$

On the other hand, we have the identity

$$\frac{\partial}{\partial \tau} \int_{x_{j-1}(\tau)}^{x_j(\tau)} F(\tau, x) dx = \int_{x_{j-1}(\tau)}^{x_j(\tau)} \frac{\partial F}{\partial \tau}(\tau, x) dx + F(\tau, x_j(\tau)) \dot{x}_j(\tau) - F(\tau, x_{j-1}(\tau)) \dot{x}_{j-1}(\tau), \tag{37}$$

where $\dot{x}_j(t) = dx_j(t)/dt$. Using this identity, we can transform the first term on the left-hand side of Eq. (35) as

$$\begin{aligned}
 \int_t^{t+\Delta t} \int_{x_{j-1}(\tau)}^{x_j(\tau)} \frac{\partial F}{\partial \tau} dx d\tau &= \int_t^{t+\Delta t} \frac{\partial}{\partial \tau} \int_{x_{j-1}(\tau)}^{x_j(\tau)} F(\tau, x) dx d\tau \\
 &\quad - \int_t^{t+\Delta t} [F(\tau, x_j(\tau)) \dot{x}_j(\tau) - F(\tau, x_{j-1}(\tau)) \dot{x}_{j-1}(\tau)] d\tau \\
 &= \int_{x_{j-1}(t+\Delta t)}^{x_j(t+\Delta t)} F(t + \Delta t, x) dx - \int_{x_{j-1}(t)}^{x_j(t)} F(t, x) dx \\
 &\quad - \int_t^{t+\Delta t} [F(\tau, x_j(\tau)) \dot{x}_j(\tau) - F(\tau, x_{j-1}(\tau)) \dot{x}_{j-1}(\tau)] d\tau. \tag{38}
 \end{aligned}$$

With the middle point $x_{j-1/2}(t)$ between $x_{j-1}(t)$ and $x_j(t)$, the first two integrals in the last line of Eq. (38) are approximated as

$$\begin{aligned}
 &\int_{x_{j-1}(t+\Delta t)}^{x_j(t+\Delta t)} F(t + \Delta t, x) dx - \int_{x_{j-1}(t)}^{x_j(t)} F(t, x) dx \\
 &\simeq F(t + \Delta t, x_{j-1/2}(t + \Delta t)) [x_j(t + \Delta t) - x_{j-1}(t + \Delta t)] \\
 &\quad - F(t, x_{j-1/2}(t)) [x_j(t) - x_{j-1}(t)]. \tag{39}
 \end{aligned}$$

The last integral in the last line of Eq. (38) is approximated as

$$\begin{aligned}
 &\int_t^{t+\Delta t} [F(\tau, x_j(\tau)) \dot{x}_j(\tau) - F(\tau, x_{j-1}(\tau)) \dot{x}_{j-1}(\tau)] d\tau \\
 &\simeq F(t, x_j(t)) [x_j(t + \Delta t) - x_j(t)] - F(t, x_{j-1}(t)) [x_{j-1}(t + \Delta t) - x_{j-1}(t)]. \tag{40}
 \end{aligned}$$

Let us denote by t_k the discretized time variable. If the time step is uniform, $t_{k+1} = t_k + \Delta t$ for any k . We use the following notation:

$$x_i^k = x_i(t_k), \quad x_w^k = x_w(t_k), \quad F_i^k = F(t_k, x_i^k), \quad G_i^k = G(t_k, x_i^k). \tag{41}$$

If we let $t = t_k$ and $t + \Delta t = t_{k+1}$ in Eq. (35) with the approximations (36) (the approximation in the second line) and Eqs. (38)–(40), we have the following discretized version of (31):

$$\begin{aligned}
 &F_{j-1/2}^{k+1} (x_j^{k+1} - x_{j-1}^{k+1}) - F_{j-1/2}^k (x_j^k - x_{j-1}^k) - F_j^k (x_j^{k+1} - x_j^k) + F_{j-1}^k (x_{j-1}^{k+1} - x_{j-1}^k) \\
 &\quad + (G_j^k - G_{j-1}^k) \Delta t = 0. \tag{42}
 \end{aligned}$$

From this equation, $F_{j-1/2}^{k+1}$ is expressed as

$$F_{j-1/2}^{k+1} = \frac{F_{j-1/2}^k(x_j^k - x_{j-1}^k) + F_j^k(x_j^{k+1} - x_j^k) - F_{j-1}^k(x_{j-1}^{k+1} - x_{j-1}^k)}{x_j^{k+1} - x_{j-1}^{k+1}} - \frac{G_j^k - G_{j-1}^k}{x_j^{k+1} - x_{j-1}^{k+1}} \Delta t, \quad (43)$$

in terms of F and G at the previous time step t_k . If we use the approximation in the last line of Eq. (36) instead of that in the second line, we have

$$F_{j-1/2}^{k+1} = \frac{F_{j-1/2}^k(x_j^k - x_{j-1}^k) + F_j^k(x_j^{k+1} - x_j^k) - F_{j-1}^k(x_{j-1}^{k+1} - x_{j-1}^k)}{x_j^{k+1} - x_{j-1}^{k+1}} - \frac{G(t_k, x_j^{k+1}) - G(t_k, x_{j-1}^{k+1})}{x_j^{k+1} - x_{j-1}^{k+1}} \Delta t. \quad (44)$$

Before moving on to the details for the Navier-Stokes equations, we interpret the meaning of Eq. (44). Let us consider the integral $\int_{x_{j-1}^{k+1}}^{x_j^{k+1}} F(t_k, x) dx$ and write it as

$$\int_{x_{j-1}^{k+1}}^{x_j^{k+1}} F(t_k, x) dx = \int_{x_{j-1}^k}^{x_j^k} F(t_k, x) dx + \int_{x_j^k}^{x_j^{k+1}} F(t_k, x) dx - \int_{x_{j-1}^k}^{x_{j-1}^{k+1}} F(t_k, x) dx. \quad (45)$$

We approximate this equality using the middle points as

$$F(t_k, x_{j-1/2}^{k+1})(x_j^{k+1} - x_{j-1}^{k+1}) \simeq F(t_k, x_{j-1/2}^k)(x_j^k - x_{j-1}^k) + F(t_k, x_j^k)(x_j^{k+1} - x_j^k) - F(t_k, x_{j-1}^k)(x_{j-1}^{k+1} - x_{j-1}^k). \quad (46)$$

Then we have

$$F(t_k, x_{j-1/2}^{k+1}) \simeq \frac{F_{j-1/2}^k(x_j^k - x_{j-1}^k) + F_j^k(x_j^{k+1} - x_j^k) - F_{j-1}^k(x_{j-1}^{k+1} - x_{j-1}^k)}{x_j^{k+1} - x_{j-1}^{k+1}}. \quad (47)$$

This expression is the same as the first fractional term on the right-hand side of Eq. (43) or (44). This gives an interpolation, using F_{j-1}^k , $F_{j-1/2}^k$, and F_j^k , to give the value of F at time t_k and at position $x_{j-1/2}^{k+1}$, i.e., at the middle point that is supposed to be at time t_{k+1} . In other words, it is an interpolation based on the conservation of F at $t = t_k$ when the j th cell moves from $[x_{j-1}^k, x_j^k]$ to $[x_{j-1}^{k+1}, x_j^{k+1}]$ [cf. Eq. (45)]. For later convenience, we rewrite Eqs. (44) and (47) in the following form:

$$F_{j-1/2}^{k+1} = F(t_k, x_{j-1/2}^{k+1}) - \frac{G(t_k, x_j^{k+1}) - G(t_k, x_{j-1}^{k+1})}{x_j^{k+1} - x_{j-1}^{k+1}} \Delta t, \quad (48a)$$

$$F(t_k, x_{j-1/2}^{k+1}) = \frac{F_{j-1/2}^k(x_j^k - x_{j-1}^k) + F_j^k(x_j^{k+1} - x_j^k) - F_{j-1}^k(x_{j-1}^{k+1} - x_{j-1}^k)}{x_j^{k+1} - x_{j-1}^{k+1}}. \quad (48b)$$

Then we can see that Eq. (48a) is a finite-difference version of Eq. (31). That is, if we consider Eq. (31) at point $x = x_{j-1/2}^{k+1}$ and time $t = t_k$ and if we replace $\partial F / \partial t$ with the forward difference $[F(t_{k+1}, x_{j-1/2}^{k+1}) - F(t_k, x_{j-1/2}^{k+1})] / \Delta t$ and $\partial G / \partial x$ with the central difference $[G(t_k, x_j^{k+1}) - G(t_k, x_{j-1}^{k+1})] / (x_j^{k+1} - x_{j-1}^{k+1})$, then we obtain Eq. (48a). Therefore, the scheme (48) consists of two steps: the interpolation required by grid displacement and the time marching. This method was proposed in [41,42].

Here we make some remarks on the accuracy of the scheme (48) on the basis of its derivation described in the preceding paragraph. For simplicity, let us consider $x_j^{k+1} - x_{j-1}^{k+1} \simeq x_j^k - x_{j-1}^k \simeq \Delta x$

(see Appendix C for the precise definition of Δx). By looking into the approximation (46) of Eq. (45) carefully, we see that the error terms contained in Eq. (46) consist of the terms of $O((\Delta x)^3)$, originating from the left-hand side and the first term on the right-hand side of Eq. (45), and the terms of $O(\Delta x(\Delta t)^2)$ and $O((\Delta t)^3)$, originating from the second and third terms on the right-hand side of Eq. (45) (the details are omitted for conciseness). Since the scheme is explicit, the stability condition imposes that Δt is comparable to Δx . If we set $\Delta t = c\Delta x$ with a constant $0 < c < 1$, then the errors contained in Eq. (46) become of $O((\Delta x)^3)$. Accordingly, Eq. (48b) contains a consistency error of $O((\Delta x)^2)$. Moreover, the second term on the right-hand side in Eq. (48a) is a central difference approximation of $\partial G/\partial x$ and the space derivatives in G are approximated by central differences as shown in Eq. (49) appearing later. Therefore, the error originating from the second term on the right-hand side in Eq. (48a) should be of $O((\Delta x)^2)$. In this way, the scheme (48) retains the second-order accuracy in x . This is also seen from the numerical result (see Appendix C).

B. Compressible Navier-Stokes equations

Now we are ready to apply the scheme (48) to the Navier-Stokes equations, for which F and G are listed in Eqs. (32)–(34). In this section we let h represent the macroscopic quantities, i.e., $h = \rho, v$, and T . Suppose that at time $t = t_k$ the quantities $h_{j-1}^k, h_{j-1/2}^k$ ($j = 1, \dots, N$), and h_N^k are all known. Then the procedure is as follows.

- (i) From Eqs. (32)–(34) we obtain $F_{j-1}^k, F_{j-1/2}^k$ ($j = 1, \dots, N$), and F_N^k .
- (ii) From Eq. (48b) we obtain $F(t_k, x_{j-1/2}^{k+1})$, which gives $h(t_k, x_{j-1/2}^{k+1})$.
- (iii) For $1 \leq j \leq N-1$, we obtain the values of the macroscopic quantities at the interfaces of the new cell, $h(t_k, x_j^{k+1})$, by the linear interpolation using $h(t_k, x_{j-1/2}^{k+1})$ and $h(t_k, x_{j+1/2}^{k+1})$. For $j = 0$ and N (i.e., on the boundary, $x = x_0^{k+1}$ and x_N^{k+1}), we first obtain $\rho(t_k, x_j^{k+1})$ by the linear extrapolation [i.e., $\rho(t_k, x_0^{k+1}) = 2\rho(t_k, x_{1/2}^{k+1}) - \rho(t_k, x_1^{k+1})$ and $\rho(t_k, x_N^{k+1}) = 2\rho(t_k, x_{N-1/2}^{k+1}) - \rho(t_k, x_{N-1}^{k+1})$] and then assume that $v(t_k, x_j^{k+1})$ and $T(t_k, x_j^{k+1})$ are the same as $v(t_k, x_j^k)$ and $T(t_k, x_j^k)$, respectively [i.e., $v(t_k, x_0^{k+1}) = v(t_k, x_0^k)$, $v(t_k, x_N^{k+1}) = v(t_k, x_N^k)$, $T(t_k, x_0^{k+1}) = T(t_k, x_0^k)$, and $T(t_k, x_N^{k+1}) = T(t_k, x_N^k)$].
- (iv) We obtain the pressure at the grid points $p(t_k, x_j^{k+1})$ and that at the cell centers $p(t_k, x_{j-1/2}^{k+1})$ by the equation of state $p = \rho T$.
- (v) We update the macroscopic quantities at the cell centers by the discrete equation (48a): We obtain $F_{j-1/2}^{k+1}$ and thus $h_{j-1/2}^{k+1}$. In this process, we use the finite difference based on the two points $x_{j-1/2}^{k+1}$ and $x_{j+1/2}^{k+1}$ (the central difference when the size of the cells is uniform) for $\partial v/\partial x$ and $\partial T/\partial x$ in G . For example, for G in Eq. (34), we use the following $G(t_k, x_j^{k+1})$:

$$\begin{aligned}
 G(t_k, x_j^{k+1}) = & \left\{ \rho(t_k, x_j^{k+1}) [v(t_k, x_j^{k+1})]^2 + \frac{5}{2} \rho(t_k, x_j^{k+1}) T(t_k, x_j^{k+1}) \right\} v(t_k, x_j^{k+1}) \\
 & - \frac{5}{4} \epsilon \Gamma_2 (T(t_k, x_j^{k+1})) \frac{T(t_k, x_{j+1/2}^{k+1}) - T(t_k, x_{j-1/2}^{k+1})}{x_{j+1/2}^{k+1} - x_{j-1/2}^{k+1}} \\
 & - \frac{4}{3} \epsilon \Gamma_1 (T(t_k, x_j^{k+1})) v(t_k, x_j^{k+1}) \frac{v(t_k, x_{j+1/2}^{k+1}) - v(t_k, x_{j-1/2}^{k+1})}{x_{j+1/2}^{k+1} - x_{j-1/2}^{k+1}}. \quad (49)
 \end{aligned}$$

- (vi) For $1 \leq j \leq N-1$, we obtain the interface values h_j^{k+1} by the linear interpolation using $h_{j-1/2}^{k+1}$ and $h_{j+1/2}^{k+1}$. For $j = 0$ and N (i.e., on the boundary, $x = x_0^{k+1}$ and x_N^{k+1}), we first obtain ρ_j^{k+1} by the linear extrapolation (i.e., $\rho_0^{k+1} = 2\rho_{1/2}^{k+1} - \rho_1^{k+1}$ and $\rho_N^{k+1} = 2\rho_{N-1/2}^{k+1} - \rho_{N-1}^{k+1}$) and then obtain v_j^{k+1} and T_j^{k+1} using the boundary conditions. More specifically, the boundary conditions, Eq. (27) discretized by using a one-sided finite difference for derivatives, give the following v_j^{k+1}

and T_j^{k+1} :

$$v_0^{k+1} = v_w^{k+1}, \quad (50a)$$

$$T_0^{k+1} = \frac{\frac{1}{2}\rho_0^{k+1}(x_1^{k+1} - x_0^{k+1}) + \alpha_v \epsilon (v_{1/2}^{k+1} - v_0^{k+1}) + \alpha_T \epsilon T_{1/2}^{k+1}}{\frac{1}{2}\rho_0^{k+1}(x_1^{k+1} - x_0^{k+1}) + \alpha_T \epsilon}, \quad (50b)$$

$$v_N^{k+1} = 0, \quad (50c)$$

$$T_N^{k+1} = \frac{\frac{1}{2}\rho_N^{k+1}(x_N^{k+1} - x_{N-1}^{k+1}) - \alpha_v \epsilon v_{N-1/2}^{k+1} + \alpha_T \epsilon T_{N-1/2}^{k+1}}{\frac{1}{2}\rho_N^{k+1}(x_N^{k+1} - x_{N-1}^{k+1}) + \alpha_T \epsilon}. \quad (50d)$$

(vii) We obtain the pressure p_j^{k+1} and $p_{j-1/2}^{k+1}$ by the equation of state $p = \rho T$.

The scheme (48) is conservative except that some errors are introduced by the treatment of the boundary values in process (iii). Concerning the mass conservation, we can show that the total mass of the gas between the two plates (per unit area of the plates) changes by an amount of $O((\Delta t)^2) + O((\Delta x)^2 \Delta t)$ at each time step (the details are omitted here). The second error comes from the extrapolation of the density. The numerical results seem to be consistent with this estimate and show satisfactory conservation properties as discussed in Appendix C.

VII. RESULTS OF COMPUTATION

In this section we show the results of numerical computation. We consider the cases of hard-sphere molecules [Eqs. (21a) and (28a)] and the BGK model [Eqs. (21b) and (28b)]. We recall that the problem is characterized by three dimensionless parameters: the (modified) Knudsen number ϵ [Eq. (9)], the dimensionless amplitude of the plate a_w [Eq. (7)], and the dimensionless distance between the center of the oscillation of the left plate and the right plate d [Eq. (5)].

In this paper, the computation is made for a single value of ϵ ($\epsilon = 0.1$), five values of a_w ($a_w = 0.01, 0.02, 0.05, 0.1, \text{ and } 0.5$), and various values of d in the range $d_0 \leq d \leq 3d_0$; here $d_0 = 2\pi\sqrt{5/6} = 5.7357\dots$ and its dimensional counterpart \tilde{d}_0 , i.e., $\tilde{d}_0 = d_0 L = 2\pi(5R\tilde{T}_0/3)^{1/2}/\tilde{\omega}$, is the wavelength of the sinusoidal acoustic wave with angular frequency $\tilde{\omega}$ in an inviscid (Euler) gas.

In the present computation, we use uniform grids for x_1 and uniform time steps. The basic choices of the numerical parameters N and Δt are $N = 2000$ ($d = d_0$) to 6000 ($d = 3d_0$) and $\Delta t \approx 1.9 \times 10^{-5}$ ($a_w = 0.01$ and 0.1) to 9.8×10^{-6} or 4.9×10^{-6} ($a_w = 0.5$). We also use coarser and finer grid systems for the accuracy tests. The details of the numerical parameters and the accuracy tests are summarized in Appendix C.

A. Profiles of macroscopic quantities

After the start of the oscillation of the left plate at $t = 0$, the plate sends out expansion and compression waves continuously. These waves interact with the waves reflected by the right plate at rest and form a complicated flow field. However, the unsteady flow field tends to converge to a time-periodic flow field after a few tens of oscillations of the plate.

In Figs. 2–6 we show the profiles of the physical quantities for hard-sphere molecules after the time-periodic state seems to have been established. Figures 2–4 show the profiles of the dimensionless density ρ , flow velocity v_1 , temperature T , and pressure p over a period $199 < t/2\pi \leq 200$ (i.e., at $t/2\pi = 199.1, 199.2, \dots, 200$) for $\epsilon = 0.1$ and $d = d_0$: Fig. 2 is for $a_w = 0.01$, Fig. 3 for $a_w = 0.1$, and Fig. 4 for $a_w = 0.5$. It should be noted that ρ , T , and p need corrections inside the Knudsen layers, which extend over $0 \leq x_1 - x_w(t) \lesssim 0.3$ and $0 \leq d - x_1 \lesssim 0.3$, in order to give correct density, temperature, and pressure, as discussed in Appendix B 4. These corrections are omitted in Figs. 2–6 and Fig. 7 appearing later.

In the case of a small amplitude (and small Mach number) (Fig. 2), the profile of v_1 [Fig. 2(b)], which is fixed at zero on the stationary plate, exhibits a structure similar to a standing wave with a

UNSTEADY MOTION OF A SLIGHTLY RAREFIED GAS ...

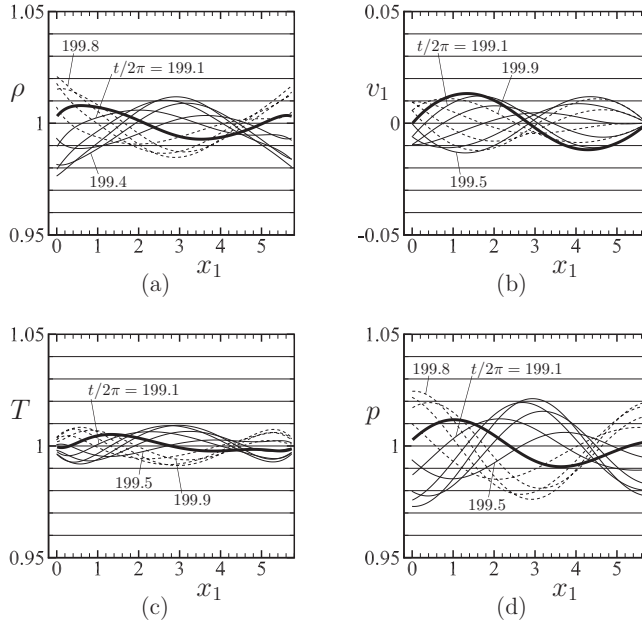


FIG. 2. Profiles of (a) ρ , (b) v_1 , (c) T , and (d) p in the time interval $199 < t/2\pi \leq 200$ for $\epsilon = 0.1$, $a_w = 0.01$, and $d = d_0$ (hard-sphere molecules). The thin solid lines indicate the profiles at $t/2\pi = 199.1, 199.2, \dots, 199.5$, the dashed lines indicate those at $t/2\pi = 199.6, 199.7, \dots, 199.9$, and the thick solid line indicates the profile at $t/2\pi = 200$.

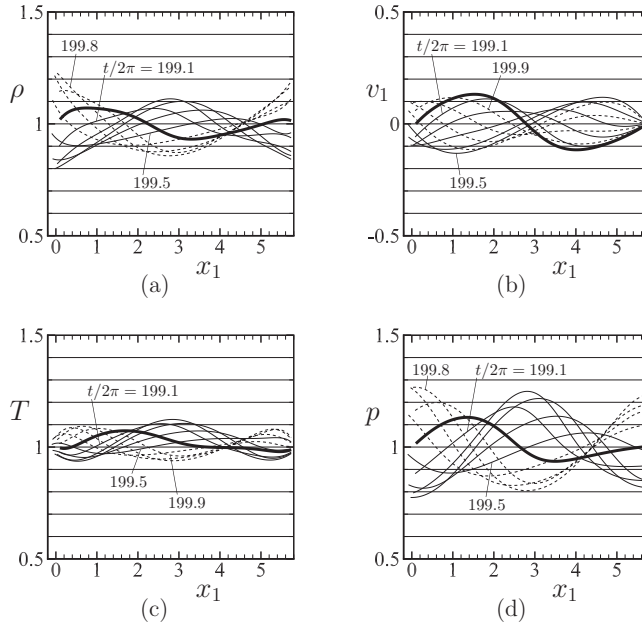


FIG. 3. Profiles of (a) ρ , (b) v_1 , (c) T , and (d) p in the time interval $199 < t/2\pi \leq 200$ for $\epsilon = 0.1$, $a_w = 0.1$, and $d = d_0$ (hard-sphere molecules). See the caption of Fig. 2 for definitions of the lines.

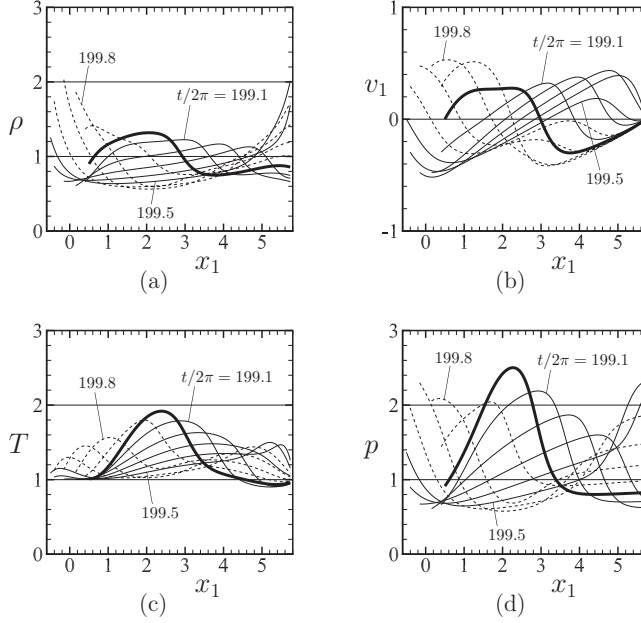


FIG. 4. Profiles of (a) ρ , (b) v_1 , (c) T , and (d) p in the time interval $199 < t/2\pi \leq 200$ for $\epsilon = 0.1$, $a_w = 0.5$, and $d = d_0$ (hard-sphere molecules). See the caption of Fig. 2 for definitions of the lines.

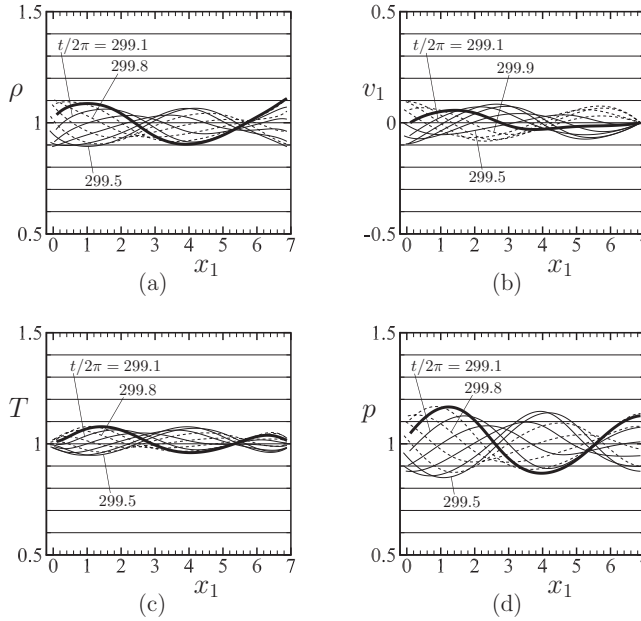


FIG. 5. Profiles of (a) ρ , (b) v_1 , (c) T , and (d) p in the time interval $299 < t/2\pi \leq 300$ for $\epsilon = 0.1$, $a_w = 0.1$, and $d = 1.2d_0$ (hard-sphere molecules). The thin solid lines indicate the profiles at $t/2\pi = 299.1, 299.2, \dots, 299.5$, the dashed lines indicate those at $t/2\pi = 299.6, 299.7, \dots, 299.9$, and the thick solid line indicates the profile at $t/2\pi = 300$.

UNSTEADY MOTION OF A SLIGHTLY RAREFIED GAS ...

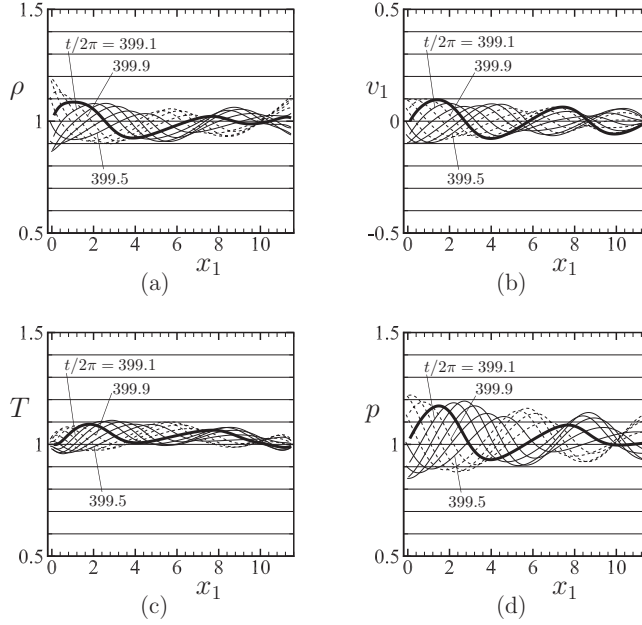


FIG. 6. Profiles of (a) ρ , (b) v_1 , (c) T , and (d) p in the time interval $399 < t/2\pi \leq 400$ for $\epsilon = 0.1$, $a_w = 0.1$, and $d = 2d_0$ (hard-sphere molecules). The thin solid lines indicate the profiles at $t/2\pi = 399.1, 399.2, \dots, 399.5$, the dashed lines indicate those at $t/2\pi = 399.6, 399.7, \dots, 399.9$, and the thick solid line indicates the profile at $t/2\pi = 400$.

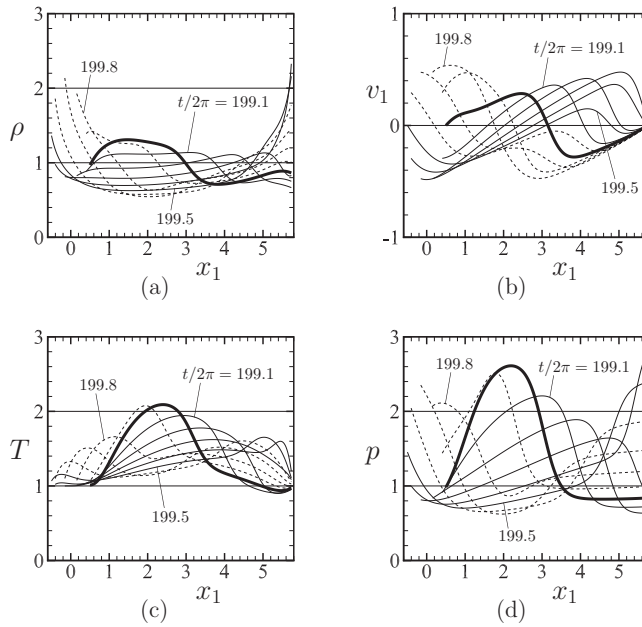


FIG. 7. Profiles of (a) ρ , (b) v_1 , (c) T , and (d) p in the time interval $199 < t/2\pi \leq 200$ for $\epsilon = 0.1$, $a_w = 0.5$, and $d = d_0$ (the BGK model). The thin solid lines indicate the profiles at $t/2\pi = 199.1, 199.2, \dots, 199.5$, the dashed lines indicate those at $t/2\pi = 199.6, 199.7, \dots, 199.9$, and the thick solid line indicates the profile at $t/2\pi = 200$.

node and two antinodes and it is close to sinusoidal curves at $t/2\pi = 199.5$ and 200. The profiles of ρ , T , and p roughly show the two-node structure with a clearer nodelike point closer to the stationary plate ($x_1 \approx 4.4$). This standing-wave-like structure with nodelike and antinodelike points is less clear for a larger amplitude (Fig. 3), though v_1 still retains the structure [Fig. 3(b)]. For a large amplitude (Fig. 4), for which the nonlinearity becomes significant, the profiles deviate from the standing-wave-like profile and no nodelike or antinodelike point is observed. In this case, ρ increases almost up to twice the initial density ($\rho = 1$) on the two plates, but decreases down to 60% of it in the middle of the gas. The T becomes almost twice the initial temperature (and the plate temperature) in the middle of the gas. There is a significant temperature jump on the resting plate because of the steep gradient of T and that of v_1 there [cf. Eq. (27b)].

Figures 5 and 6 show the profiles at $\epsilon = 0.1$ and $a_w = 0.1$ but for different d : $d = 1.2d_0$ (Fig. 5) and $2d_0$ (Fig. 6). For a slightly wider gap between the two plates (Fig. 5), the feature of the profile changes from that of Fig. 3. The standing-wave-like structure becomes less clear for v_1 but clearer for ρ , T , and p . In particular, ρ and T exhibit profiles with two nodelike points and three antinodelike points rather clearly [Figs. 5(a) and 5(c)]. On the other hand, for $d = 2d_0$ (Fig. 6), the standing-wave-like structure is clear (in particular, in the right half of the gas region) only for v_1 [Fig. 6(b)]. This difference between the profile of v_1 and those of ρ , T , and p is due to the difference in constraint on the plates. The v_1 takes the imposed values on the plate [cf. Eq. (27)], which corresponds to the fixed-end condition for a standing wave, whereas no constraint is imposed on ρ on the plates, which corresponds to the free-end condition for a standing wave. The condition for the temperature on the plates is somewhat intermediate, since the jump condition (27) does not fix the values completely. Of course, the situation is not so simple because there is the viscous dissipation and v_1 , ρ , and T are not independent but interact nonlinearly. Nevertheless, some behavior of the profiles may be understood from these properties. For instance, the oscillating plate inputs kinetic energy into the gas, so the velocity field is affected by the plate most directly. In the cases of $d = d_0$ (Fig. 3) and $2d_0$ (Fig. 6), the standing-wave-like profile of v_1 is observed, as mentioned above. For $d = d_0$, the amplitude of v_1 in the gas exceeds the input amplitude $a_w = 0.1$ in the gas [Fig. 3(b)] in spite of the fact that the viscous dissipation should decay the amplitude. This amplification is caused by a sort of resonance (see the last paragraph in Sec. VII B). It is also observed for $d = 2d_0$ [Fig. 6(b)]. In this case, because of the wider gas region, the waves attenuate more. Nevertheless, the amplitude of v_1 reaches almost the input value 0.1 in the gas. For $d = 1.2d_0$ [Fig. 5(b)], the amplitude of v_1 is smaller than the input value.

In Fig. 7, the profiles corresponding to Fig. 4 ($\epsilon = 0.1$, $a_w = 0.5$, and $d = d_0$) are shown for the BGK model. They are qualitatively the same as those in Fig. 4, but the maximum values of the density and temperature during one period is larger.

B. Momentum and energy transfer

Let us denote by $\tilde{\mathcal{P}}^L$ and $\tilde{\mathcal{P}}^R$ the \tilde{x}_1 component of the momentum transferred from the left (oscillating) plate to the gas and that transferred from the gas to the right (resting) plate per unit area and per unit time, respectively. We also denote by $\tilde{\mathcal{E}}^L$ and $\tilde{\mathcal{E}}^R$ the energy transferred from the left plate to the gas and that from the gas to the right plate, respectively. Then we define their dimensionless counterparts \mathcal{P}^L , \mathcal{P}^R , \mathcal{E}^L , and \mathcal{E}^R by

$$\mathcal{P}^L = \tilde{\mathcal{P}}^L / \tilde{p}_0, \quad \mathcal{P}^R = \tilde{\mathcal{P}}^R / \tilde{p}_0, \quad \mathcal{E}^L = \tilde{\mathcal{E}}^L / \tilde{p}_0 \tilde{c}_0, \quad \mathcal{E}^R = \tilde{\mathcal{E}}^R / \tilde{p}_0 \tilde{c}_0. \quad (51)$$

If we neglect the terms of $O(\epsilon^2)$, they are expressed in the following form:

$$\mathcal{P}^L(t) = \left(p - \frac{4}{3} \epsilon \Gamma_1 \frac{\partial v_1}{\partial x_1} \right)_{x_1=x_w(t)}, \quad (52a)$$

$$\mathcal{P}^R(t) = \left(p - \frac{4}{3} \epsilon \Gamma_1 \frac{\partial v_1}{\partial x_1} \right)_{x_1=d}, \quad (52b)$$

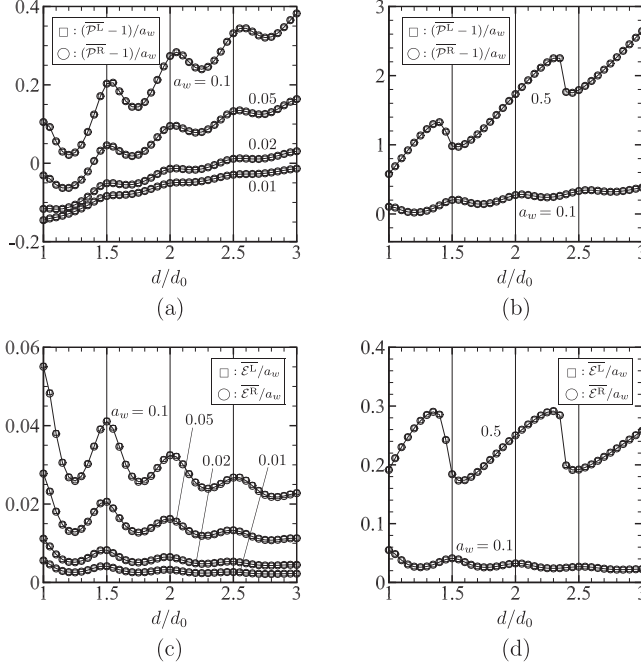


FIG. 8. Average momentum and energy transfer over a period at the time-periodic state for $\epsilon = 0.1$ and some a_w (hard-sphere molecules): (a) and (b) $(\overline{\mathcal{P}}^L - 1)/a_w$ and $(\overline{\mathcal{P}}^R - 1)/a_w$ vs d/d_0 and (c) and (d) $\overline{\mathcal{E}}^L/a_w$ and $\overline{\mathcal{E}}^R/a_w$ vs d/d_0 . The results shown are at $t/2\pi = 200$ for $1 \leq d/d_0 \leq 2$, at $t/2\pi = 400$ for $2 < d/d_0 \leq 2.5$, and at $t/2\pi = 600$ for $2.5 < d/d_0 \leq 3$.

$$\mathcal{E}^L(t) = \left[\left(p - \frac{4}{3}\epsilon\Gamma_1 \frac{\partial v_1}{\partial x_1} \right) v_w(t) - \frac{5}{4}\epsilon\Gamma_2 \frac{\partial T}{\partial x_1} \right]_{x_1=x_w(t)}, \quad (52c)$$

$$\mathcal{E}^R(t) = \left(-\frac{5}{4}\epsilon\Gamma_2 \frac{\partial T}{\partial x_1} \right)_{x_1=d}. \quad (52d)$$

These formulas are not subject to the Knudsen-layer corrections, as discussed in Appendix B 4. In addition, we introduce the time average of \mathcal{P}^L , \mathcal{P}^R , \mathcal{E}^L , and \mathcal{E}^R over one period from $t - 2\pi$ to t and denote them by an overline, i.e.,

$$\overline{\mathcal{W}}(t) = \frac{1}{2\pi} \int_{t-2\pi}^t \mathcal{W}(t') dt', \quad (53)$$

where \mathcal{W} stands for \mathcal{P}^L , \mathcal{P}^R , \mathcal{E}^L , or \mathcal{E}^R .

Figures 8 and 9 show $(\overline{\mathcal{P}}^L - 1)/a_w$, $(\overline{\mathcal{P}}^R - 1)/a_w$, $\overline{\mathcal{E}}^L/a_w$, and $\overline{\mathcal{E}}^R/a_w$ at a long time, for which the time-periodic state seems to have been reached, versus d/d_0 at $\epsilon = 0.1$ for several values of a_w : Fig. 8 is for hard-sphere molecules and Fig. 9 for the BGK model. The results shown are at $t/2\pi = 200$ for $1 \leq d/d_0 \leq 2$, at $t/2\pi = 400$ for $2 < d/d_0 \leq 2.5$, and at $t/2\pi = 600$ for $2.5 < d/d_0 \leq 3$. As is seen from the figures, $\overline{\mathcal{P}}^L = \overline{\mathcal{P}}^R$ and $\overline{\mathcal{E}}^L = \overline{\mathcal{E}}^R$ hold. This also indicates that the time-periodic state has been established. If \mathcal{P}^L , \mathcal{P}^R , \mathcal{E}^L , and \mathcal{E}^R make a sinusoidal oscillation in time with period 2π as in the case of linear setting, $\overline{\mathcal{P}}^L - 1$, $\overline{\mathcal{P}}^R - 1$, $\overline{\mathcal{E}}^L$, and $\overline{\mathcal{E}}^R$ all vanish. In fact, when a_w is small ($a_w = 0.01$), these quantities are very small. For $a_w = 0.01$, $\overline{\mathcal{P}}^L - 1$ and $\overline{\mathcal{P}}^R - 1$ are negative for all $d/d_0 (\leq 3)$ in Fig. 8 and for $d/d_0 \lesssim 2$ in Fig. 9. This is because the average distance between the plates after a long time is d , which is longer than the initial distance $d - a_w$. Therefore, the

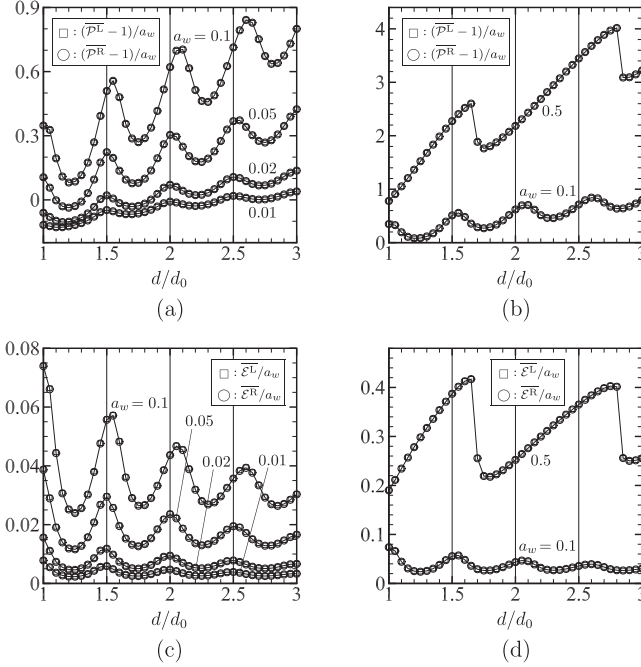


FIG. 9. Average momentum and energy transfer over a period at the time-periodic state for $\epsilon = 0.1$ and some a_w (the BGK model): (a) and (b) $(\overline{\mathcal{P}}^L - 1)/a_w$ and $(\overline{\mathcal{P}}^R - 1)/a_w$ vs d/d_0 and (c) and (d) $\overline{\mathcal{E}}^L/a_w$ and $\overline{\mathcal{E}}^R/a_w$ vs d/d_0 . The results shown are at $t/2\pi = 200$ for $1 \leq d/d_0 \leq 2$, at $t/2\pi = 400$ for $2 < d/d_0 \leq 2.5$, and at $t/2\pi = 600$ for $2.5 < d/d_0 \leq 3$.

stationary plate is pulled (relative to the pressure exerted on the plate in the initial equilibrium state) by the gas and the same is true for the oscillating plate. As d increases, the difference between d and $d - a_w$ becomes small, so the pulling effect becomes small. Indeed, $\overline{\mathcal{P}}^L - 1$ and $\overline{\mathcal{P}}^R - 1$ are closer to zero for larger d/d_0 . When the amplitude (and the Mach number) a_w becomes large ($a_w = 0.01 \rightarrow 0.5$), $\overline{\mathcal{P}}^L - 1$ and $\overline{\mathcal{P}}^R - 1$ become positive and larger and $\overline{\mathcal{E}}^L$ and $\overline{\mathcal{E}}^R$ also increase. In other words, when a_w is not small, the stationary plate is pushed outward (i.e., in the positive x_1 direction), on average, by the oscillating plate via the gas. The stationary plate also receives the energy (for all d), on average, from the oscillating plate via the gas. The mechanism of this average momentum and energy transfer is explained in view of the interaction of the gas molecules with the moving plate in [21] (see Sec. 3.3 in [21]). Therefore, we do not repeat it here. If there is no stationary plate that receives the positive momentum relative to the initial pressure ($\overline{\mathcal{P}}^R - 1 > 0$), the gas flows in the x_1 direction, i.e., toward infinity. This flow is called the acoustic stream [43,44].

It is seen from Figs. 8 and 9 that both $\overline{\mathcal{P}}^L$ (or $\overline{\mathcal{P}}^R$) and $\overline{\mathcal{E}}^L$ (or $\overline{\mathcal{E}}^R$) exhibit local maxima and minima almost periodically with respect to d/d_0 . When a_w is small, the period is almost equal to $d_0/2$, that is, these quantities take local maxima near $d/d_0 = n/2$ with integer n and local minima near $d/d_0 = n/2 + 1/4$. For larger values of a_w ($a_w = 0.1 \rightarrow 0.5$), the period tends to increase.

The appearance of the local maxima at $d/d_0 \approx n/2$ for small a_w is reasonable for the following reason. Let us consider a column of an inviscid (or Euler) gas and a sinusoidal sound wave propagating along the column. If the column has reflective ends and its length is a multiple of $d_0/2 = \pi(5RT_0/3)^{1/2}/\tilde{\omega}$, the natural frequency of the column coincides with $\tilde{\omega}$. That is, a sinusoidal standing wave may be formed, and if one of the ends oscillates sinusoidally with angular frequency $\tilde{\omega}$, the amplitude of the standing wave is amplified. In other words, the resonance takes place. If there is no energy dissipation, the amplitude increases indefinitely. In a real gas, however, the energy

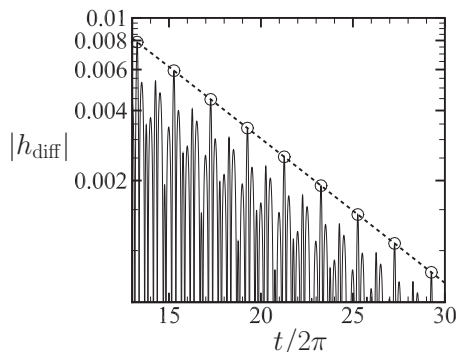


FIG. 10. Schematic for $|h_{\text{diff}}|$ vs t . The circles indicate the peaks, each of which corresponds to the maximum after the previous peak.

dissipates and escapes from the column in the form of heat through the ends, so the amplitude remains finite even in the case of resonance, i.e., even when $d/d_0 \approx n/2$. Nevertheless, the amplitude in these cases is still larger than that for other d . In other words, more energy and momentum are transmitted to the gas in this situation. This roughly explains the appearance of the local maxima at $d/d_0 \approx n/2$ when the amplitude of the oscillation of the plate a_w is small.

C. Approach to the time-periodic state

As mentioned in Sec. VII A, the motion of the gas approaches a time-periodic state as time proceeds. In this section we investigate the speed of approach to the time-periodic state. We consider the case of $\epsilon = 0.1$, $a_w = 0.1$, and $d = d_0$ and regard the numerical solution for $199 < t/2\pi \leq 200$ as the time-periodic solution. For any given time t , an integer n and a number $\tau \in (0, 2\pi]$ such that $t = (n - 1)2\pi + \tau$ are uniquely determined, i.e., $n - 1$ is the maximum integer that is smaller than $t/2\pi$. Then we define the difference between the solution at time t and the time-periodic solution by

$$h_{\text{diff}}(t, x_1) = h(t, x_1) - h(199 \times 2\pi + \tau, x_1), \quad (54)$$

where h represents the macroscopic quantities, i.e., $h = \rho, v_1, T$, and p . Obviously, $h(199 \times 2\pi + \tau, x_1)$ ($0 < \tau \leq 2\pi$) indicates our time-periodic solution. If we plot $|h_{\text{diff}}|$ at a fixed x_1 as a function of t , it is oscillatory, as is shown schematically in Fig. 10. Therefore, we pick up the peaks indicated by circles in the figure. Each of these peaks corresponds to the maximum after the previous peak and can be picked up by the following procedure.

- (i) We first prepare the time-series data of all local maxima of $|h_{\text{diff}}|$.
- (ii) We compare one of the local maxima with the next one. If the former maximum is smaller than the latter, we remove the former one from the time-series data.
- (iii) We repeat step (ii) until there is no local maximum to be removed.

In Fig. 11 we show the curves joining the peaks thus obtained in semilogarithmic scale for $x_1 = a_w = 0.1$ [Fig. 11(a)], $x_1 = (a_w + d)/2 = (0.1 + d_0)/2 = 2.9178 \dots$ [Fig. 11(b)], and $x_1 = d = d_0 = 5.7357 \dots$ [Fig. 11(c)] [v_1 is excluded in Fig. 11(c) because $v_1 = 0$ at $x_1 = d$]. For all ρ, v_1, T , and p and at all three points, the curve tends to approach a straight line after the initial stage and the gradients of all lines are almost the same for each of the hard-sphere molecules and the BGK model. If we denote the function corresponding to the curve by $F(t, x_1)$, then we have $|h_{\text{diff}}(t, x_1)| \leq F(t, x_1)$ and $\log_{10} F(t, x_1) \approx -\alpha' t + \beta'$, with α' and β' being constants. This is equivalent to writing

$$|h_{\text{diff}}(t, x_1)| \leq F(t, x_1) \approx C \exp(-\alpha t) \quad \text{for } t \gg 1, \quad (55)$$

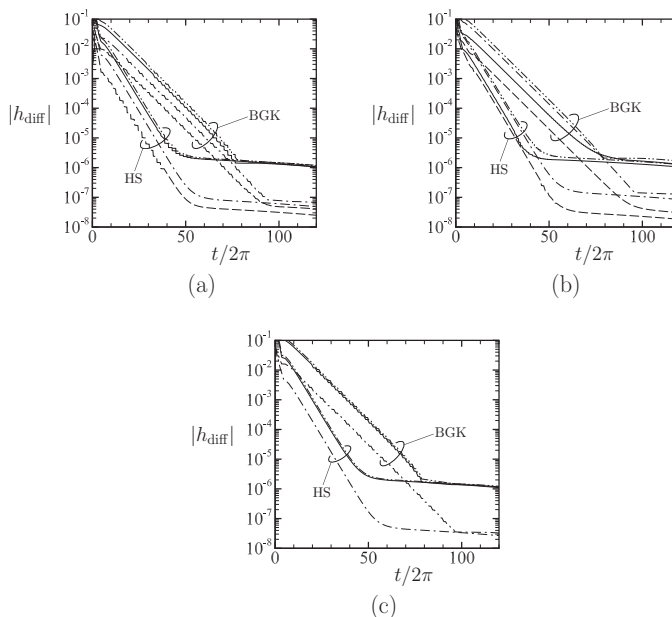


FIG. 11. Curves joining the peaks obtained by steps (i)–(iii) of the procedure for $\epsilon = 0.1$, $a_w = 0.1$, and $d = d_0$ at (a) $x_1 = a_w = 0.1$, (b) $x_1 = (a_w + d)/2 = (0.1 + d_0)/2 = 2.9178\dots$, and (c) $x_1 = d = d_0 = 5.7357\dots$. The solid lines indicate $|\rho_{\text{diff}}|$, the dashed lines $|v_{\text{diff}}|$, the dash-dotted lines $|T_{\text{diff}}|$, and the dash-double-dotted lines $|p_{\text{diff}}|$. The curve of $|v_{\text{diff}}|$ is excluded in (c) because $v_1 = 0$ at $x_1 = d$.

where C and α ($= \alpha' \ln 10 = \alpha' \times 2.302585\dots$) are constants and α is seemingly independent of x_1 and the physical quantities but dependent on the molecular model. The approach to the time-periodic state is faster for hard-sphere molecules. The curves of $F(t, x_1)$ cease to decrease when $F(t, x_1)$ becomes 10^{-5} – 10^{-7} . This is probably because the computation has reached the limit of accuracy. In fact, we have confirmed that the part for the exponential decay extends for finer space grids and time steps. We now pick up the interval of t in which each curve corresponding to $F(t, x_1)$ seems to be a straight line, that is, we take the interval $10 < t/2\pi \leq 30$ for hard-sphere molecules and $20 < t/2\pi \leq 50$ for the BGK model. Then, for this interval, we construct an approximate straight line, by the least-squares method, for each of ρ , v_1 , T , and p and for each of the three points of x_1 as well as two additional points $x_1 = (3a_w + d)/4 = (0.3 + d_0)/4$ and $x_1 = (a_w + 3d)/4 = (0.1 + 3d_0)/4$. As a result, the gradient $-\alpha'$ of the curve of $\log_{10} F$ is obtained as -1.65×10^{-2} (9 cases out of 19 cases), -1.64×10^{-2} (6 cases), -1.66×10^{-2} (2 cases), -1.62×10^{-2} (1 case), and -1.67×10^{-2} (1 case) for hard-sphere molecules and -9.8×10^{-3} (7 cases out of 19 cases), -9.9×10^{-3} (5 cases), -10.0×10^{-3} (3 cases), -9.7×10^{-3} (2 cases), and -10.1×10^{-3} (2 cases) for the BGK model. Therefore, we can conclude that the factor α in Eq. (55) is approximately given as $\alpha = 3.80 \times 10^{-2}$ for hard-sphere molecules and $\alpha = 2.26 \times 10^{-2}$ for the BGK model.

VIII. CONCLUSION

In the present paper we investigated the unsteady motion of a rarefied gas between two parallel plates caused when one of the plates starts a harmonic oscillation in its normal direction. We considered the case where the speed of oscillation of the plate is not necessarily small compared to the sonic speed (i.e., fully nonlinear setting), but the Knudsen number is small. Therefore, as an alternative to the Boltzmann or its model equations, for which accurate numerical computation for a long time is difficult for small Knudsen numbers, we decided to use the compressible Navier-Stokes equations and slip boundary conditions. However, it was practically impossible to find appropriate

slip (or jump) boundary conditions for the compressible Navier-Stokes equations that can be applied immediately to the present problem. For example, one can find formulas for slip boundary conditions for compressible Navier-Stokes equations in [37]. However, the boundary is assumed to be at rest and the numerical values of the coefficients in the formulas are not given. Therefore, we revisited this classical problem and derived the correct temperature jump condition for the present problem (Appendix B).

After we had prepared the boundary condition, we solved the compressible Navier-Stokes system numerically by a method suitable for the present problem containing a plate moving in its normal direction (Sec. VI). The result shows that the flow field approaches the time-periodic state after a few tens of oscillations of the plate. The properties of this time-periodic state were investigated in detail (Secs. VII B and VII C). When the speed of oscillation of the plate is not very small compared to the sonic speed, the momentum in the outward direction and the energy, averaged over a period, is transmitted to the stationary plate by the oscillating plate (Sec. VII B). This confirms the earlier result [21] based on the BGK model for the intermediate Knudsen numbers, though the computation there was carried out until shorter times.

ACKNOWLEDGMENTS

This work was partially supported by the AYAME Program between JSPS and Inria and by the Grant-in-aid No. 26630051 from JSPS. One of the authors (K.A.) wishes to thank National Center for Theoretical Sciences, National Taiwan University and Department of Mathematics, National Cheng Kung University for their support and hospitality. He also thanks Prof. Luc Mieussens, Dr. Céline Baranger, Dr. Julien Mathiaud, and Dr. Giorgio Martalò for useful discussions about the slip boundary conditions.

APPENDIX A: BOLTZMANN COLLISION INTEGRAL

In this Appendix we summarize the collision integral and related matters on the basis of [25]. Thus, the notation here basically follows that in [25] (see Sec. 1.9 and Appendix A in [25]). However, since we avoided using a caret to indicate dimensionless quantities in the main text, there are some differences in notation. For instance, $[f, g, J(f, g)]$ in this appendix correspond to $[\hat{f}, \hat{g}, \hat{J}(\hat{f}, \hat{g})]$ in [25]. In addition, we occasionally use boldface to indicate vectors and a centered dot the scalar product, e.g., $\boldsymbol{\zeta} = \zeta_i$ and $\boldsymbol{\alpha} \cdot (\boldsymbol{\zeta}_* - \boldsymbol{\zeta}) = \alpha_j(\zeta_{*j} - \zeta_j)$, here and in Appendix B.

1. Collision operators

We start with the definition of the bilinear form $J(f, g)$:

$$J(f, g) = \frac{1}{2} \int_{\boldsymbol{\zeta}_* \in \mathbb{R}^3, \boldsymbol{\alpha} \in \mathbb{S}^2} (f' g'_* + f'_* g' - f g_* - f_* g) \hat{B} d\Omega(\boldsymbol{\alpha}) d\boldsymbol{\zeta}_*. \quad (\text{A1})$$

Here we used the convention, i.e., $f = f(\boldsymbol{\zeta})$, $f_* = f(\boldsymbol{\zeta}_*)$, $f' = f(\boldsymbol{\zeta}')$, $f'_* = f(\boldsymbol{\zeta}'_*)$, and the same for g ; $\boldsymbol{\zeta}$, which was denoted by ζ_i in the main text, is the dimensionless molecular velocity; when a pair of molecules with velocities $\boldsymbol{\zeta}$ and $\boldsymbol{\zeta}_*$ collide, the velocities of the respective molecules after collision $\boldsymbol{\zeta}'$ and $\boldsymbol{\zeta}'_*$ are expressed as

$$\boldsymbol{\zeta}' = \boldsymbol{\zeta} + [\boldsymbol{\alpha} \cdot (\boldsymbol{\zeta}_* - \boldsymbol{\zeta})] \boldsymbol{\alpha}, \quad \boldsymbol{\zeta}'_* = \boldsymbol{\zeta}_* - [\boldsymbol{\alpha} \cdot (\boldsymbol{\zeta}_* - \boldsymbol{\zeta})] \boldsymbol{\alpha}, \quad (\text{A2})$$

where $\boldsymbol{\alpha}$ is the unit vector in the direction of $\boldsymbol{\zeta}' - \boldsymbol{\zeta}$; $d\boldsymbol{\zeta}_* = d\zeta_{*1} d\zeta_{*2} d\zeta_{*3}$ and $d\Omega(\boldsymbol{\alpha})$ is the solid-angle element around $\boldsymbol{\alpha}$; \hat{B} is a non-negative function of $|\boldsymbol{\alpha} \cdot (\boldsymbol{\zeta}_* - \boldsymbol{\zeta})|/|\boldsymbol{\zeta}_* - \boldsymbol{\zeta}|$ and $|\boldsymbol{\zeta}_* - \boldsymbol{\zeta}|$, i.e.,

$$\hat{B} = \hat{B} \left(\frac{|\boldsymbol{\alpha} \cdot (\boldsymbol{\zeta}_* - \boldsymbol{\zeta})|}{|\boldsymbol{\zeta}_* - \boldsymbol{\zeta}|}, |\boldsymbol{\zeta}_* - \boldsymbol{\zeta}| \right), \quad (\text{A3})$$

which depends on the intermolecular potential, and $\hat{B} = |\boldsymbol{\alpha} \cdot (\boldsymbol{\zeta}_* - \boldsymbol{\zeta})|/4\sqrt{2\pi}$ for hard-sphere molecules (see Sec. 1.9 and Appendix A in [25] for the details of \hat{B} , noting that \hat{B} here is the same as \hat{B} in [25]).

According to Sec. 1.9 in [25], the mean collision frequency \bar{v}_{c0} and the mean free path l_0 in the equilibrium state at rest with density $\bar{\rho}_0$ and temperature \bar{T}_0 are, respectively, expressed as

$$\bar{v}_{c0} = (\bar{\rho}_0/m)B_0, \quad l_0 = (2/\sqrt{\pi})\bar{c}_0/\bar{v}_{c0} = (2/\sqrt{\pi})\bar{c}_0/(\bar{\rho}_0/m)B_0, \quad (\text{A4})$$

where B_0 is defined by

$$B_0 = \frac{1}{\bar{\rho}_0^2} \int \tilde{f}_0(\tilde{\boldsymbol{\zeta}}) \tilde{f}_0(\tilde{\boldsymbol{\zeta}}_*) B \left(\frac{|\boldsymbol{\alpha} \cdot (\tilde{\boldsymbol{\zeta}}_* - \tilde{\boldsymbol{\zeta}})|}{|\tilde{\boldsymbol{\zeta}}_* - \tilde{\boldsymbol{\zeta}}|}, |\tilde{\boldsymbol{\zeta}}_* - \tilde{\boldsymbol{\zeta}}| \right) d\Omega(\boldsymbol{\alpha}) d\tilde{\boldsymbol{\zeta}} d\tilde{\boldsymbol{\zeta}}_*. \quad (\text{A5})$$

Here $\tilde{f}_0(\tilde{\boldsymbol{\zeta}})$ is the dimensional Maxwellian with density $\bar{\rho}_0$, velocity 0, and temperature \bar{T}_0 , i.e., $\tilde{f}_0(\tilde{\boldsymbol{\zeta}}) = \bar{\rho}_0(2\pi R\bar{T}_0)^{-3/2} \exp(-|\tilde{\boldsymbol{\zeta}}|^2/2R\bar{T}_0)$, and B is the dimensional counterpart of \hat{B} appearing in the dimensional form of the Boltzmann collision integral. In fact, \hat{B} is defined by $\hat{B} = B/B_0$. For hard-sphere molecules with diameter d_m ,

$$\bar{v}_{c0} = 2\sqrt{2\pi}\bar{c}_0 d_m^2 (\bar{\rho}_0/m), \quad l_0 = 1/\sqrt{2\pi} d_m^2 (\bar{\rho}_0/m). \quad (\text{A6})$$

When the intermolecular potential extends to infinity, the integral in Eq. (A5) generally diverges. See Sec. 1.9 in [25] for the treatment in such a case.

The linearized collision operator $\mathcal{L}(\cdot)$ is defined by

$$\begin{aligned} \mathcal{L}(\varphi) &= 2J(E, E\varphi)/E \\ &= \int E(\zeta_*) (\varphi'_* + \varphi' - \varphi_* - \varphi) \hat{B} \left(\frac{|(\boldsymbol{\zeta}_* - \boldsymbol{\zeta}) \cdot \boldsymbol{\alpha}|}{|\boldsymbol{\zeta}_* - \boldsymbol{\zeta}|}, |\boldsymbol{\zeta}_* - \boldsymbol{\zeta}| \right) d\Omega(\boldsymbol{\alpha}) d\boldsymbol{\zeta}_*, \end{aligned} \quad (\text{A7})$$

where $\zeta_* = (\zeta_{*1}^2 + \zeta_{*2}^2 + \zeta_{*3}^2)^{1/2}$, $E(\cdot)$ is the function defined by Eq. (16b), and the same convention as in Eq. (A1) is used, i.e., $\varphi_* = \varphi(\boldsymbol{\zeta}_*)$, $\varphi' = \varphi(\boldsymbol{\zeta}')$, etc. Now we introduce the following extended linearized collision operator $\mathcal{L}_a(\cdot)$:

$$\mathcal{L}_a(\varphi) = \int E(\zeta_*) (\varphi'_* + \varphi' - \varphi_* - \varphi) \hat{B}_a \left(\frac{|(\boldsymbol{\zeta}_* - \boldsymbol{\zeta}) \cdot \boldsymbol{\alpha}|}{|\boldsymbol{\zeta}_* - \boldsymbol{\zeta}|}, |\boldsymbol{\zeta}_* - \boldsymbol{\zeta}| \right) d\Omega(\boldsymbol{\alpha}) d\boldsymbol{\zeta}_*, \quad (\text{A8})$$

where

$$\hat{B}_a = \hat{B}_a \left(\frac{|\boldsymbol{\alpha} \cdot (\boldsymbol{\zeta}_* - \boldsymbol{\zeta})|}{|\boldsymbol{\zeta}_* - \boldsymbol{\zeta}|}, |\boldsymbol{\zeta}_* - \boldsymbol{\zeta}| \right) = \frac{1}{\sqrt{a}} \hat{B} \left(\frac{|\boldsymbol{\alpha} \cdot (\boldsymbol{\zeta}_* - \boldsymbol{\zeta})|}{|\boldsymbol{\zeta}_* - \boldsymbol{\zeta}|}, \sqrt{a} |\boldsymbol{\zeta}_* - \boldsymbol{\zeta}| \right) \quad (\text{A9})$$

and a is a positive quantity independent of $\boldsymbol{\zeta}$. Obviously, $\mathcal{L}_1(\varphi) = \mathcal{L}(\varphi)$ holds, and for hard-sphere molecules, $\mathcal{L}_a(\varphi) = \mathcal{L}(\varphi)$ holds.

For the BGK model, the dimensionless collision integral $J(f, f)$ in Eq. (8) is replaced by the following $J_{\text{BGK}}(f)$:

$$J_{\text{BGK}}(f) = \rho(f_e - f), \quad (\text{A10})$$

where f_e is a local Maxwellian

$$f_e = \frac{\rho}{(\pi T)^{3/2}} \exp \left(-\frac{(\zeta_i - v_i)^2}{T} \right) \quad (\text{A11})$$

and ρ , v_i , and T are defined by Eq. (3a). In this model, the collision frequency ν_c of a molecule with velocity $\tilde{\zeta}_i$ depends neither on $\tilde{\zeta}_i$ nor on the shape of \tilde{f} and is assumed to be $A_c \bar{\rho}$, where A_c is a constant. This corresponds to the Maxwell molecules in which the intermolecular potential is proportional to $1/r^4$, with r the distance between two molecules. Therefore, the mean collision

frequency \bar{v}_{c0} and the mean free path l_0 in the equilibrium state at rest with density $\bar{\rho}_0$ and temperature \bar{T}_0 become

$$\bar{v}_{c0} = A_c \bar{\rho}_0, \quad l_0 = (2/\sqrt{\pi}) \bar{c}_0 / A_c \bar{\rho}_0. \quad (\text{A12})$$

The linearized collision operators $\mathcal{L}_{a\text{BGK}}(\cdot)$ and $\mathcal{L}_{\text{BGK}}(\cdot)$ for the BGK model, which correspond to $\mathcal{L}_a(\cdot)$ and $\mathcal{L}(\cdot)$, respectively, take the forms

$$\sqrt{a} \mathcal{L}_{a\text{BGK}}(\varphi) = \int \left[1 + 2\boldsymbol{\zeta} \cdot \boldsymbol{\zeta}_* + \frac{2}{3} \left(\zeta^2 - \frac{3}{2} \right) \left(\zeta_*^2 - \frac{3}{2} \right) \right] \varphi(\boldsymbol{\zeta}_*) E(\zeta_*) d\boldsymbol{\zeta}_* - \varphi(\boldsymbol{\zeta}), \quad (\text{A13a})$$

$$\mathcal{L}_{\text{BGK}}(\varphi) = \mathcal{L}_{1\text{BGK}}(\varphi), \quad (\text{A13b})$$

where $\zeta = (\zeta_1^2 + \zeta_2^2 + \zeta_3^2)^{1/2}$.

2. Functions \mathcal{A} and $\mathcal{B}^{(0)}$

The functions $\mathcal{A}(C, T)$ and $\mathcal{B}^{(0)}(C, T)$ occurring in the first-order term of the Chapman-Enskog solution (15) are defined as follows: $\mathcal{A}(\zeta, a)$ is the solution of the integral equation

$$\mathcal{L}_a[\zeta_i \mathcal{A}(\zeta, a)] = -\zeta_i \left(\zeta^2 - \frac{5}{2} \right), \quad (\text{A14})$$

with the subsidiary condition

$$\int_0^\infty \zeta^4 \mathcal{A}(\zeta, a) E(\zeta) d\zeta = 0, \quad (\text{A15})$$

and the function $\mathcal{B}^{(0)}(\zeta, a)$ is the solution of the integral equation

$$\mathcal{L}_a \left[\left(\zeta_i \zeta_j - \frac{1}{3} \zeta^2 \delta_{ij} \right) \mathcal{B}^{(0)}(\zeta, a) \right] = -2 \left(\zeta_i \zeta_j - \frac{1}{3} \zeta^2 \delta_{ij} \right). \quad (\text{A16})$$

In [25], $\mathcal{A}(\zeta, 1)$ is denoted by $A(\zeta)$ and $\mathcal{B}^{(0)}(\zeta, 1)$ by $B(\zeta)$:

$$\mathcal{A}(\zeta, 1) = A(\zeta), \quad \mathcal{B}^{(0)}(\zeta, 1) = B(\zeta). \quad (\text{A17})$$

Thus, for hard-sphere molecules, $\mathcal{A}(\zeta, a) = A(\zeta)$ and $\mathcal{B}^{(0)}(\zeta, a) = B(\zeta)$ for any a . The numerical values of $A(\zeta)$ and $B(\zeta)$ for hard-sphere molecules are tabulated in Table 3.1 of [25] (see also [45,46]). These numerical data make it possible to perform numerical integration of the integrals in Eq. (19) and give Γ_1 and Γ_2 shown in Eq. (21a) [46]. For the BGK model, Eqs. (A14) [with Eq. (A15)] and (A16), with $\mathcal{L}_a = \mathcal{L}_{a\text{BGK}}$, give the solutions

$$\mathcal{A}(\zeta, a) = \sqrt{a} \left(\zeta^2 - \frac{5}{2} \right), \quad \mathcal{B}^{(0)}(\zeta, a) = 2\sqrt{a}, \quad (\text{A18})$$

which give Γ_1 and Γ_2 shown in Eq. (21b).

APPENDIX B: DERIVATION OF THE JUMP BOUNDARY CONDITIONS

In this Appendix we give an outline of the derivation of the jump boundary conditions (27). The method of analysis is basically based on the asymptotic theory developed by Sone (see, e.g., [25]). Therefore, the method itself is not new. However, the results that will be presented here are new in the sense that they are not found in [25].

1. Knudsen layer: Equation

We restrict ourselves to the derivation of the condition (27a) on the oscillating plate. From the result, the condition (27b) on the resting plate is derived immediately. Let us consider Eq. (26) near the moving plate $x_1 = x_w(t)$. Then Φ is appreciable only in the thin layer of thickness of the order of ϵ adjacent to the plate. If we substitute Eq. (26) into the Boltzmann equation (8) and note the fact

that

$$\frac{\partial f_{\text{CE}}^{(1)}}{\partial t} + \zeta_1 \frac{\partial f_{\text{CE}}^{(1)}}{\partial x_1} = \frac{1}{\epsilon} J(f_{\text{CE}}^{(1)}, f_{\text{CE}}^{(1)}) + O(\epsilon), \quad (\text{B1})$$

we have

$$\epsilon \left(\frac{\partial f^{(0)} \Phi}{\partial t} + \zeta_1 \frac{\partial f^{(0)} \Phi}{\partial x_1} \right) = 2J(f_{\text{CE}}^{(1)}, f^{(0)} \Phi) + \epsilon J(f^{(0)} \Phi, f^{(0)} \Phi) + O(\epsilon). \quad (\text{B2})$$

Further, if we note that

$$\frac{\partial f^{(0)} \Phi}{\partial t} + \zeta_1 \frac{\partial f^{(0)} \Phi}{\partial x_1} = f^{(0)} \left(\frac{\partial \Phi}{\partial t} + \zeta_1 \frac{\partial \Phi}{\partial x_1} \right) + \Phi f^{(0)} O(1), \quad (\text{B3a})$$

$$2J(f_{\text{CE}}^{(1)}, f^{(0)} \Phi) = 2J(f^{(0)}, f^{(0)} \Phi) + \epsilon f^{(0)} O(\Phi), \quad (\text{B3b})$$

Eq. (B2) is transformed to

$$\frac{\partial \Phi}{\partial t} + \zeta_1 \frac{\partial \Phi}{\partial x_1} = \frac{1}{\epsilon f^{(0)}} 2J(f^{(0)}, f^{(0)} \Phi) + O(\Phi). \quad (\text{B4})$$

Let us introduce the new coordinate system $(\hat{t}, \eta, \hat{\zeta}_1, \hat{\zeta}_2, \hat{\zeta}_3)$ by

$$\hat{t} = t, \quad \epsilon \eta = x_1 - x_w(t), \quad \hat{\zeta}_1 = \zeta_1 - v_w(t), \quad \hat{\zeta}_2 = \zeta_2, \quad \hat{\zeta}_3 = \zeta_3 \quad (\text{B5})$$

and change the variables from $(t, x_1, \zeta_1, \zeta_2, \zeta_3)$ to $(\hat{t}, \eta, \hat{\zeta}_1, \hat{\zeta}_2, \hat{\zeta}_3)$. More specifically, we write

$$\Phi(t, x_1, \zeta_1, \zeta_2, \zeta_3) = \hat{\Phi}(\hat{t}, \eta, \hat{\zeta}_1, \hat{\zeta}_2, \hat{\zeta}_3) \quad (\text{B6})$$

and assume that

$$\frac{\partial \hat{\Phi}}{\partial \eta} = O(\hat{\Phi}), \quad \hat{\Phi} \rightarrow 0 \text{ (rapidly) as } \eta \rightarrow \infty. \quad (\text{B7})$$

Then the left-hand side of (B4) becomes

$$\frac{\partial \hat{\Phi}}{\partial \hat{t}} + \frac{1}{\epsilon} \hat{\zeta}_1 \frac{\partial \hat{\Phi}}{\partial \eta} - \dot{v}_w(\hat{t}) \frac{\partial \hat{\Phi}}{\partial \hat{\zeta}_1}. \quad (\text{B8})$$

On the other hand, Eq. (A1) gives, with the same convention,

$$2J(f^{(0)}, f^{(0)} \Phi) (f^{(0)})^{-1} = \int f_*^{(0)} (\Phi'_* + \Phi' - \Phi_* - \Phi) \hat{B} \left(\frac{|(\zeta_* - \zeta) \cdot \alpha|}{|\zeta_* - \zeta|}, |\zeta_* - \zeta| \right) d\Omega(\alpha) d\zeta_*, \quad (\text{B9})$$

where

$$f_*^{(0)} = \frac{\rho}{(\pi T)^{3/2}} \exp \left(-\frac{(\zeta_{*1} - v_1)^2 + \zeta_{*2}^2 + \zeta_{*3}^2}{T} \right), \quad (\text{B10})$$

and the fact that $f^{(0)'} f_*^{(0)'} = f^{(0)} f_*^{(0)}$ has been used. We consider the range of η for which Φ is appreciable, i.e., $\eta = O(1)$. Then, for $h = \rho$, v_1 , and T , we can write

$$h = h(\hat{t}, x_w(\hat{t}) + \epsilon \eta) = h_B(\hat{t}) + O(\epsilon \eta), \quad (\text{B11})$$

where $h_B(\hat{t}) \equiv h(\hat{t}, x_w(\hat{t}))$ indicates the value on the plate. If we assume Eq. (25), then from Eq. (B11) we have

$$\rho = \rho_B(\hat{t}) + O(\epsilon \eta), \quad v_1 = v_w(\hat{t}) + O(\epsilon(\eta + 1)), \quad T = 1 + O(\epsilon(\eta + 1)). \quad (\text{B12})$$

Therefore, $f_*^{(0)}$ can be expressed as

$$f_*^{(0)} = \frac{\rho_B}{\pi^{3/2}} \exp \left\{ - [(\zeta_{*1} - v_w)^2 + \zeta_{*2}^2 + \zeta_{*3}^2] \right\} [1 + O(\epsilon(\eta + 1))] = \rho_B E(\hat{\zeta}_*) [1 + O(\epsilon(\eta + 1))]. \quad (\text{B13})$$

In the last expression, the new variable $\hat{\zeta}_i$ [Eq. (B5)] and $E(\cdot)$ defined in Eq. (16b) are used; more specifically, $\hat{\zeta}_{*i}$ is defined by Eq. (B5) with $\zeta_i = \zeta_{*i}$ and $\hat{\zeta}_* = (\hat{\zeta}_{*1}^2 + \hat{\zeta}_{*2}^2 + \hat{\zeta}_{*3}^2)^{1/2}$. With this expression, Eq. (B9) can be expressed in terms of the new variables as

$$2J(f^{(0)}, f^{(0)}\Phi)(f^{(0)})^{-1} = \rho_B \int E(\hat{\zeta}_*)(\hat{\Phi}'_* + \hat{\Phi}' - \hat{\Phi}_* - \hat{\Phi}) \times \hat{B} \left(\frac{|\hat{\zeta}_* - \hat{\zeta}| \cdot \boldsymbol{\alpha}}{|\hat{\zeta}_* - \hat{\zeta}|}, |\hat{\zeta}_* - \hat{\zeta}| \right) d\Omega(\boldsymbol{\alpha}) d\hat{\zeta}_* + O(\epsilon(\eta + 1)\hat{\Phi}), \quad (\text{B14})$$

where $\hat{\zeta}'_i$ and $\hat{\zeta}'_{*i}$ are defined by Eq. (B5) with $\zeta_i = \zeta'_i$ and $\zeta_i = \zeta'_{*i}$, respectively, so that $\hat{\zeta}_i, \hat{\zeta}_{*i}, \hat{\zeta}'_i$, and $\hat{\zeta}'_{*i}$ satisfy the same relations as Eq. (A2). In Eq. (B14), the same convention is used: More specifically, $\hat{\Phi} = \hat{\Phi}(\hat{t}, \eta, \hat{\zeta}_i)$, $\hat{\Phi}_* = \hat{\Phi}(\hat{t}, \eta, \hat{\zeta}_{*i})$, $\hat{\Phi}' = \hat{\Phi}(\hat{t}, \eta, \hat{\zeta}'_i)$, and $\hat{\Phi}'_* = \hat{\Phi}(\hat{t}, \eta, \hat{\zeta}'_{*i})$.

In summary, Eqs. (B8) and (B14) lead to the following expression of Eq. (B4):

$$\hat{\zeta}_1 \frac{\partial \hat{\Phi}}{\partial \eta} = \rho_B \mathcal{L}(\hat{\Phi}) + O(\epsilon(\eta + 1)\hat{\Phi}), \quad (\text{B15})$$

where the linearized collision operator defined by Eq. (A7) is used, i.e.,

$$\mathcal{L}(\hat{\Phi}) = \int E(\hat{\zeta}_*)(\hat{\Phi}'_* + \hat{\Phi}' - \hat{\Phi}_* - \hat{\Phi}) \hat{B} \left(\frac{|\hat{\zeta}_* - \hat{\zeta}| \cdot \boldsymbol{\alpha}}{|\hat{\zeta}_* - \hat{\zeta}|}, |\hat{\zeta}_* - \hat{\zeta}| \right) d\Omega(\boldsymbol{\alpha}) d\hat{\zeta}_*. \quad (\text{B16})$$

Since $\hat{\Phi}$ vanishes rapidly as $\eta \rightarrow \infty$, the term of $O(\epsilon(\eta + 1)\hat{\Phi})$ in Eq. (B15), which is of $O(\epsilon)$ for finite η , vanishes rapidly as $\eta \rightarrow \infty$. If we neglect this term, introduce a new coordinate y by

$$y = \rho_B \eta, \quad (\text{B17})$$

and define

$$\hat{\Phi}(\hat{t}, \eta, \hat{\zeta}_i) = \phi(\hat{t}, y, \hat{\zeta}_i), \quad (\text{B18})$$

then we have the following equation for ϕ :

$$\hat{\zeta}_1 \frac{\partial \phi}{\partial y} = \mathcal{L}(\phi) \quad (0 < y < \infty). \quad (\text{B19})$$

2. Knudsen layer: Boundary condition

Next we derive the boundary conditions for Eq. (B19). The velocity distribution function of the form of Eq. (26) has to satisfy the boundary condition on the plate, Eq. (10a), that is,

$$f_B^{(0)}(1 + \Psi_B \epsilon + \Phi_B \epsilon) = \frac{\sigma_w}{\pi^{3/2}} \exp \left(- [(\zeta_1 - v_w(t))^2 + \zeta_2^2 + \zeta_3^2] \right) \quad \text{for } \zeta_1 - v_w(t) > 0, \quad (\text{B20a})$$

$$\sigma_w = -2\pi^{1/2} \int_{\zeta_1 - v_w(t) < 0} [\zeta_1 - v_w(t)] f_B^{(0)}(1 + \Psi_B \epsilon + \Phi_B \epsilon) d\boldsymbol{\zeta}, \quad (\text{B20b})$$

where the subscript B indicates the value on the plate, i.e., at $x_1 = x_w(t)$ or $\eta = 0$, and the terms of $O(\epsilon^2)$ are omitted.

Now we recall Eq. (25a), i.e., $v_{1B} - v_w(t) = O(\epsilon)$ and $T_B - 1 = O(\epsilon)$, and let

$$v_{1B} - v_w(t) = \check{v}_1 \epsilon, \quad T_B - 1 = \check{T} \epsilon. \quad (\text{B21})$$

Then $\check{v}_1 = O(1)$ and $\check{T} = O(1)$. By expanding v_{1B} around $v_w(t)$ and T_B around 1 in $f_B^{(0)}$ and Ψ_B , the boundary value $f_B^{(0)}(1 + \Psi_B \epsilon)$ is expressed in the form

$$f_B^{(0)}(1 + \Psi_B \epsilon) = \rho_B E(\hat{\zeta}) \left[1 + 2\hat{\zeta}_1 \check{v}_1 \epsilon + \left(\hat{\zeta}^2 - \frac{3}{2} \right) \check{T} \epsilon - \frac{1}{\rho_B} \left(\hat{\zeta}_1^2 - \frac{1}{3} \hat{\zeta}^2 \right) \left(\frac{\partial v_1}{\partial x_1} \right)_B \mathcal{B}^{(0)}(\hat{\zeta}, 1) \epsilon - \frac{1}{\rho_B} \hat{\zeta}_1 \left(\frac{\partial T}{\partial x_1} \right)_B \mathcal{A}(\hat{\zeta}, 1) \epsilon + O(\epsilon^2) \right], \quad (\text{B22})$$

where the variable $\hat{\zeta}_i$ [Eq. (B5)] and $E(\cdot)$ [Eq. (16b)] are used and $\hat{\zeta} = (\hat{\zeta}_1^2 + \hat{\zeta}_2^2 + \hat{\zeta}_3^2)^{1/2}$. If we use this expression in the integrand in Eq. (B20b) and carry out possible integrations, we have the following expression for σ_w :

$$\sigma_w = \rho_B [1 + \delta \epsilon + O(\epsilon^2)], \quad (\text{B23a})$$

$$\delta = -\sqrt{\pi} \check{v}_1 + \frac{1}{2} \check{T} - \frac{1}{3\rho_B} \left(\frac{\partial v_1}{\partial x_1} \right)_B \int_0^\infty r^5 \mathcal{B}^{(0)}(r, 1) e^{-r^2} dr - 2\sqrt{\pi} \int_{\hat{\zeta}_1 < 0} \hat{\zeta}_1 \Phi_B E(\hat{\zeta}) d\hat{\zeta}. \quad (\text{B23b})$$

Let us note that

$$\Phi_B = \Phi(t, x_w(t), \zeta_i) = \hat{\Phi}(\hat{t}, \eta = 0, \hat{\zeta}_i) = \phi(\hat{t}, y = 0, \hat{\zeta}_i). \quad (\text{B24})$$

Then Eq. (B20), together with Eqs. (B22)–(B24), gives the boundary condition for ϕ on the plate, that is,

$$\begin{aligned} \phi(\hat{t}, y = 0, \hat{\zeta}_i) &= - (2\hat{\zeta}_1 + \sqrt{\pi}) \check{v}_1 - (\hat{\zeta}^2 - 2) \check{T} \\ &+ \left[-\frac{1}{3} \int_0^\infty r^5 \mathcal{B}(r) e^{-r^2} dr + \left(\hat{\zeta}_1^2 - \frac{1}{3} \hat{\zeta}^2 \right) \mathcal{B}(\hat{\zeta}) \right] \frac{1}{\rho_B} \left(\frac{\partial v_1}{\partial x_1} \right)_B \\ &+ \hat{\zeta}_1 \mathcal{A}(\hat{\zeta}) \frac{1}{\rho_B} \left(\frac{\partial T}{\partial x_1} \right)_B - 2\sqrt{\pi} \int_{\hat{\zeta}_{*1} < 0} \hat{\zeta}_{*1} \phi(\hat{t}, y = 0, \hat{\zeta}_{*i}) E(\hat{\zeta}_{*}) d\hat{\zeta}_{*} \quad \text{for } \hat{\zeta}_1 > 0. \end{aligned} \quad (\text{B25})$$

Here the terms of $O(\epsilon)$ have been neglected and $\mathcal{A}(\hat{\zeta}, 1)$ and $\mathcal{B}^{(0)}(\hat{\zeta}, 1)$ have been replaced by $\mathcal{A}(\hat{\zeta})$ and $\mathcal{B}(\hat{\zeta})$ [cf. Eq. (A17)]. In addition, because of Eq. (B7), ϕ should vanish rapidly as $y \rightarrow \infty$, i.e.,

$$\phi \rightarrow 0 \quad \text{as } y \rightarrow \infty. \quad (\text{B26})$$

Equations (B25) and (B26) form the boundary conditions for Eq. (B19).

3. Jump boundary conditions

Before analyzing Eqs. (B19), (B25), and (B26), we integrate Eq. (B19) multiplied by $E(\hat{\zeta})$ with respect to $\hat{\zeta}_i$ over its whole space. Then we have

$$\frac{\partial}{\partial y} \int \hat{\zeta}_1 \phi E(\hat{\zeta}) d\hat{\zeta} = 0, \quad (\text{B27})$$

since the integral of $\mathcal{L}(\phi)$ vanishes. Because of Eq. (B26),

$$\int \hat{\zeta}_1 \phi E(\hat{\zeta}) d\hat{\zeta} = 0 \quad (\text{B28})$$

holds for any y . Therefore, we have

$$\int \hat{\zeta}_1 \phi(\hat{t}, y = 0, \hat{\zeta}_i) E(\hat{\zeta}) d\hat{\zeta} = 0. \quad (\text{B29})$$

On the other hand, the boundary condition (10a) satisfies the impermeability condition

$$\int [\zeta_1 - v_w(t)] f_B d\hat{\zeta} = \int \hat{\zeta}_1 f_B^{(0)} [1 + \Psi_B \epsilon + \Phi_B \epsilon + O(\epsilon^2)] d\hat{\zeta} = 0. \quad (\text{B30})$$

Since $f_B^{(0)} = \rho_B E(\hat{\zeta}) [1 + O(\epsilon)]$ and $\Phi_B = \phi(\hat{t}, y = 0, \hat{\zeta}_i)$ [Eq. (B24)], Eqs. (B29) and (B30) give the relation

$$\int \hat{\zeta}_1 f_B^{(0)} (1 + \Psi_B \epsilon) d\hat{\zeta} = O(\epsilon^2). \quad (\text{B31})$$

Using Eq. (B22), performing the integration, and noting that $\int \hat{\zeta}_1^2 \mathcal{A}(\hat{\zeta}, 1) E(\hat{\zeta}) d\hat{\zeta} = 0$, we obtain the relation

$$\check{v}_1 = [v_{1B} - v_w(t)]/\epsilon = O(\epsilon). \quad (\text{B32})$$

Therefore, we can neglect \check{v}_1 in Eq. (B25).

The mathematical structure of the solution of the half-space boundary-value problem, Eqs. (B19), (B25), and (B26), is discussed in [25] on the basis of the theorem conjectured in [47], proved in [48], and further analyzed in [49] (the reader is also referred to the more recent overview in [50]). In the present case, where $\check{v}_1 = 0$ in Eq. (B25), the unique solution exists when \check{T} is related to $(1/\rho_B)(\partial v_1/\partial x_1)_B$ and $(1/\rho_B)(\partial T/\partial x_1)_B$ appropriately. This relation, which we will obtain below, gives the boundary condition for the temperature.

Let us set

$$\phi = \frac{1}{\rho_B} \left(\frac{\partial v_1}{\partial x_1} \right)_B \phi_v + \frac{1}{\rho_B} \left(\frac{\partial T}{\partial x_1} \right)_B \phi_T, \quad (\text{B33a})$$

$$\check{T} = \frac{1}{\rho_B} \left(\frac{\partial v_1}{\partial x_1} \right)_B \alpha_v + \frac{1}{\rho_B} \left(\frac{\partial T}{\partial x_1} \right)_B \alpha_T \quad (\text{B33b})$$

and insert them in Eqs. (B19), (B25) (with $\check{v}_1 = 0$), and (B26). Then, because of the linearity of the problem, we obtain the equations and boundary conditions for ϕ_v and ϕ_T : For ϕ_v the equation and boundary conditions are

$$\hat{\zeta}_1 \frac{\partial \phi_v(\hat{t}, y, \hat{\zeta})}{\partial y} = \mathcal{L}[\phi_v(\hat{t}, y, \hat{\zeta})], \quad (\text{B34a})$$

$$\begin{aligned} \phi_v(\hat{t}, 0, \hat{\zeta}) &= -2\sqrt{\pi} \int_{\hat{\zeta}_{*1} < 0} \hat{\zeta}_{*1} \phi_v(\hat{t}, 0, \hat{\zeta}_*) E(\hat{\zeta}_*) d\hat{\zeta}_* - \alpha_v (\hat{\zeta}^2 - 2) \\ &\quad - \frac{1}{3} \int_0^\infty r^5 B(r) e^{-r^2} dr + \left(\hat{\zeta}_1^2 - \frac{1}{3} \hat{\zeta}^2 \right) B(\hat{\zeta}) \quad (\hat{\zeta}_1 > 0), \end{aligned} \quad (\text{B34b})$$

$$\phi_v(\hat{t}, y, \hat{\zeta}) \rightarrow 0 \quad (y \rightarrow \infty) \quad (\text{B34c})$$

and for ϕ_T they are

$$\hat{\zeta}_1 \frac{\partial \phi_T(\hat{t}, y, \hat{\zeta})}{\partial y} = \mathcal{L}[\phi_T(\hat{t}, y, \hat{\zeta})], \quad (\text{B35a})$$

$$\phi_T(\hat{t}, 0, \hat{\zeta}) = -2\sqrt{\pi} \int_{\hat{\zeta}_{*1} < 0} \hat{\zeta}_{*1} \phi_T(\hat{t}, 0, \hat{\zeta}_*) E(\hat{\zeta}_*) d\hat{\zeta}_* - \alpha_T (\hat{\zeta}^2 - 2) + \hat{\zeta}_1 A(\hat{\zeta}) \quad (\hat{\zeta}_1 > 0), \quad (\text{B35b})$$

$$\phi_T(\hat{t}, y, \hat{\zeta}) \rightarrow 0 \quad (y \rightarrow \infty). \quad (\text{B35c})$$

The undetermined constants α_v and α_T are determined together with the solutions ϕ_v and ϕ_T , respectively.

Problem for ϕ_T . The problem for ϕ_T , Eq. (B35), is exactly the same as the classical temperature jump problem (see, e.g., [27,51–54]). For hard-sphere molecules, the problem was

solved numerically in [54] (see also [46]). We note that $(y, \hat{\zeta}_i, \phi_T, \alpha_T)$ (here) is equal to $(x_1, \zeta_i, \Phi_K, \beta)$ (in [54]), which is equal to $(\eta, \zeta_i, \Phi_1, b)$ (in [46]) and α_T (here) is equal to d_1 (in [25]; see Sec. 3.1.5 in [25]). For the BGK model, an accurate value of α_T was obtained in [55,56]: α_T (here) is equal to d_1 (in [55,56]). In summary, we have from [25] the values listed in Eq. (28), i.e., for hard-sphere molecules and the BGK model, respectively,

$$\alpha_T = 2.4001, \quad \alpha_T = 1.30272 \quad (\text{B36})$$

for the diffuse reflection.

Problem for ϕ_v . The problem for ϕ_v , Eq. (B34), has been studied rarely because it does not correspond to a specific half-space problem of physical interest. It has appeared only in the generalized slip flow theory (linear theory) with evaporation and condensation on the boundary [25,56] (the BGK model) and that for time-dependent problems with solid boundary [34–36] (hard-sphere molecules). For instance, $(y, \hat{\zeta}_1, \phi_v, \alpha_v)$ (here) is equal to $(\eta, \mu\zeta, \phi_5, c_5^{(0)})$ (in [35]) and α_v (here) is equal to $(4/3)d_6$ in [25,56]. To summarize, we have, from [35] for hard-sphere molecules and from [25] for the BGK model, the values of α_v listed in Eq. (28), i.e., for hard-sphere molecules and the BGK model, respectively,

$$\alpha_v = 0.45957, \quad \alpha_v = 0.44045 \quad (\text{B37})$$

for the diffuse reflection.

In summary, Eqs. (B21), (B32), and (B33b) give v_{1B} and T_B in the form

$$v_{1B} - v_w(t) = 0, \quad T_B - 1 = \frac{1}{\rho_B} \left(\frac{\partial v_1}{\partial x_1} \right)_B \alpha_v \epsilon + \frac{1}{\rho_B} \left(\frac{\partial T}{\partial x_1} \right)_B \alpha_T \epsilon, \quad (\text{B38})$$

where the term of $O(\epsilon^2)$ in Eq. (B21) has been neglected. With the values of α_v and α_T mentioned above, these relations give the boundary conditions for the Navier-Stokes equations on the oscillating plate, i.e., at $x_1 = x_w(t)$ [see Eq. (27a)]. The boundary conditions on the plate at rest, i.e., at $x_1 = d$, are obtained by replacing (x_1, v_1, v_w) with $(d - x_1, -v_1, 0)$ in Eq. (B38) [see Eq. (27b)] and noting that the subscript B indicates the values at $x_1 = d$.

4. Macroscopic quantities inside the Knudsen layer

Let h stand for any of the macroscopic quantities ρ , v_i , T , p , p_{ij} , and q_i in this section. The general relation between the velocity distribution function f and h is given by Eqs. (3a) and (3b). For convenience in the following discussion, we use subscript CE to indicate h associated with the Chapman-Enskog solution $f_{\text{CE}}^{(1)}$. To be more specific, h_{CE} (or ρ_{CE} , $v_{\text{CE}i}$, T_{CE} , p_{CE} , $p_{\text{CE}ij}$, and $q_{\text{CE}i}$) in this section is equal to h (or ρ , v_i , T , p , p_{ij} , and q_i) appearing in Secs. IV–VII and in Appendixes B 1–B 3. The Chapman-Enskog solution is subject to the correction inside the Knudsen layer [cf. Eq. (26)] to provide the correct solution there. We rewrite Eq. (26) in the following form, using the subscript tot to indicate the correct solution inside the Knudsen layer:

$$f_{\text{tot}} = f_{\text{CE}}^{(1)} + f^{(0)}\Phi + O(\epsilon^2) = f^{(0)}(1 + \Psi\epsilon + \Phi\epsilon) + O(\epsilon^2), \quad (\text{B39})$$

where it is noted that the macroscopic quantities contained in $f^{(0)}$ are h_{CE} . Now we denote the correct macroscopic quantities inside the Knudsen layer by h_{tot} and express it as

$$h_{\text{tot}} = h_{\text{CE}} + h_{\text{K}}^{(1)}\epsilon + O(\epsilon^2). \quad (\text{B40})$$

In other words, this provides the definition of $h_{\text{K}}^{(1)}$.

We derive $h_{\text{K}}^{(1)}$ in the Knudsen layer at the oscillating plate [$x_1 = x_w(t)$]. The corresponding result in the Knudsen layer at the resting plate ($x_1 = d$) can be obtained immediately. We substitute Eqs. (B39) and (B40) into the general relations (3a) and (3b) (with $f = f_{\text{tot}}$ and $h = h_{\text{tot}}$) and take into account that $f_{\text{CE}}^{(1)}$ and h_{CE} also satisfy Eqs. (3a) and (3b). Then we simplify the expressions by

using Eq. (B12) for h_{CE} contained in the factors multiplied by Φ and neglect the terms of $O(\epsilon^2)$. After changing the integration variables from ζ_i to $\hat{\zeta}_i$ (thus changing from Φ to ϕ) [cf. Eqs. (B5), (B6), and (B18)], we obtain the following expressions of $h_{\text{K}}^{(1)}$:

$$\rho_{\text{K}}^{(1)} = (\rho_{\text{CE}})_B \int \phi E(\hat{\zeta}) d\hat{\zeta}, \quad v_{\text{K}i}^{(1)} = \int \hat{\zeta}_i \phi E(\hat{\zeta}) d\hat{\zeta}, \quad (\text{B41a})$$

$$T_{\text{K}}^{(1)} = \frac{2}{3} \int \left(\hat{\zeta}_j^2 - \frac{3}{2} \right) \phi E(\hat{\zeta}) d\hat{\zeta}, \quad p_{\text{K}}^{(1)} = (\rho_{\text{CE}})_B T_{\text{K}}^{(1)} + \rho_{\text{K}}^{(1)}, \quad (\text{B41b})$$

$$p_{\text{K}ij}^{(1)} = 2(\rho_{\text{CE}})_B \int \hat{\zeta}_i \hat{\zeta}_j \phi E(\hat{\zeta}) d\hat{\zeta}, \quad q_{\text{K}i}^{(1)} = (\rho_{\text{CE}})_B \int \hat{\zeta}_i \left(\hat{\zeta}_j^2 - \frac{5}{2} \right) \phi E(\hat{\zeta}) d\hat{\zeta}. \quad (\text{B41c})$$

From the symmetry of the problem [cf. Eq. (4)], $v_{\text{K}2}^{(1)} = v_{\text{K}3}^{(1)} = 0$, $p_{\text{K}12}^{(1)} = p_{\text{K}21}^{(1)} = p_{\text{K}23}^{(1)} = p_{\text{K}32}^{(1)} = p_{\text{K}31}^{(1)} = p_{\text{K}13}^{(1)} = 0$, and $q_{\text{K}2}^{(1)} = q_{\text{K}3}^{(1)} = 0$. Furthermore, Eq. (B28) shows that $v_{\text{K}1}^{(1)} = 0$. Integrating Eq. (B19) multiplied by $\hat{\zeta}_1 E(\hat{\zeta})$ and that multiplied by $(\hat{\zeta}_j^2 - 5/2)E(\hat{\zeta})$ with respect to $\hat{\zeta}_i$ over its whole space and repeating the argument that led to Eq. (B28), we observe that $p_{\text{K}11}^{(1)} = q_{\text{K}1}^{(1)} = 0$.

Now we remove the subscript CE and summarize the correct (nontrivial) macroscopic quantities h_{tot} inside the Knudsen layer. That is, if we neglect the terms of $O(\epsilon^2)$, we have

$$\rho_{\text{tot}} = \rho + \epsilon \rho_{\text{K}}^{(1)}, \quad v_{\text{tot}1} = v_1, \quad T_{\text{tot}} = T + \epsilon T_{\text{K}}^{(1)}, \quad p_{\text{tot}} = p + \epsilon p_{\text{K}}^{(1)}, \quad (\text{B42a})$$

$$p_{\text{tot}11} = p - \frac{4}{3} \epsilon \Gamma_1(T) \frac{\partial v_1}{\partial x_1}, \quad p_{\text{tot}22} = p + \epsilon p_{\text{K}22}^{(1)}, \quad p_{\text{tot}33} = p + \epsilon p_{\text{K}33}^{(1)}, \quad (\text{B42b})$$

$$q_{\text{tot}1} = -\frac{5}{4} \epsilon \Gamma_2(T) \frac{\partial T}{\partial x_1}, \quad (\text{B42c})$$

where

$$\rho_{\text{K}}^{(1)} = \rho_B \int \phi E(\hat{\zeta}) d\hat{\zeta}, \quad T_{\text{K}}^{(1)} = \frac{2}{3} \int \left(\hat{\zeta}_j^2 - \frac{3}{2} \right) \phi E(\hat{\zeta}) d\hat{\zeta}, \quad (\text{B43a})$$

$$p_{\text{K}}^{(1)} = \rho_B T_{\text{K}}^{(1)} + \rho_{\text{K}}^{(1)}, \quad p_{\text{K}ij}^{(1)} = 2\rho_B \int \hat{\zeta}_i \hat{\zeta}_j \phi E(\hat{\zeta}) d\hat{\zeta}. \quad (\text{B43b})$$

If we insert Eq. (B33a) in Eq. (B43a), we have

$$\rho_{\text{K}}^{(1)} = \left(\frac{\partial v_1}{\partial x_1} \right)_B \Omega_v(y) + \left(\frac{\partial T}{\partial x_1} \right)_B \Omega_T(y), \quad (\text{B44a})$$

$$T_{\text{K}}^{(1)} = \frac{1}{\rho_B} \left(\frac{\partial v_1}{\partial x_1} \right)_B \Theta_v(y) + \frac{1}{\rho_B} \left(\frac{\partial T}{\partial x_1} \right)_B \Theta_T(y), \quad (\text{B44b})$$

where

$$\Omega_v(y) = \int \phi_v E(\hat{\zeta}) d\hat{\zeta}, \quad \Omega_T(y) = \int \phi_T E(\hat{\zeta}) d\hat{\zeta}, \quad (\text{B45a})$$

$$\Theta_v(y) = \frac{2}{3} \int \left(\hat{\zeta}_j^2 - \frac{3}{2} \right) \phi_v E(\hat{\zeta}) d\hat{\zeta}, \quad \Theta_T(y) = \frac{2}{3} \int \left(\hat{\zeta}_j^2 - \frac{3}{2} \right) \phi_T E(\hat{\zeta}) d\hat{\zeta}. \quad (\text{B45b})$$

For hard-sphere molecules, $\Omega_T(y)$ and $\Theta_T(y)$ were obtained in [46,54]. More precisely, $[y, \Omega_T(y), \Theta_T(y)]$ (here) is equal to $[x_1, \Omega(x_1), \Theta(x_1)]$ (in [54]), which is equal to $[\eta, \Omega(\eta), \Theta(\eta)]$ (in [46]) and $[\eta, \Omega_1(\eta), \Theta_1(\eta)]$ (in [25]). These functions are tabulated in the respective references (see, for example, Table 3.2 in [25]). On the other hand, $\Omega_v(y)$ and $\Theta_v(y)$ were obtained in [35];

$[y, \Omega_v(y), \Theta_v(y)]$ (here) is equal to $[\eta, \Omega_5^{(0)}(\eta), \Theta_5^{(0)}(\eta)]$ (in [35]) and $\Omega_5^{(0)}(\eta)$ and $\Theta_5^{(0)}(\eta)$ are tabulated in Table 5.2 of [35].

For the BGK model, $\Omega_T(y)$ and $\Theta_T(y)$ were obtained, e.g., in [56]; $[y, \Omega_T(y), \Theta_T(y)]$ (here) is equal to $[\eta, \Omega_1(\eta), \Theta_1(\eta)]$ (in [56]), which is equal to $[\eta, \Omega_1(\eta), \Theta_1(\eta)]$ (in [25]) and these functions are tabulated in the respective references (see, for example, Table 3.3 in [25]). As for $\Omega_v(y)$ and $\Theta_v(y)$, they were also obtained in [56]; $[y, \Omega_v(y), \Theta_v(y)]$ (here) is equal to $[\eta, (4/3)\Omega_6(\eta), (4/3)\Theta_6(\eta)]$ (in [56]), which is equal to $[\eta, (4/3)\Omega_6(\eta), (4/3)\Theta_6(\eta)]$ (in [25]), and $\Omega_6(\eta)$ and $\Theta_6(\eta)$ are tabulated, for instance, in Table 3.3 in [25].

Once the data of $\Omega_v(y)$, $\Theta_v(y)$, $\Omega_T(y)$, and $\Theta_T(y)$ are obtained from the references quoted above, the correct macroscopic quantities ρ_{tot} , T_{tot} , and p_{tot} are obtained from Eqs. (B42a), (B43b), and (B44) (we omit the result of $p_{K22}^{(1)}$ and $p_{K33}^{(1)}$). We emphasize that v_{tot1} , p_{tot1} , and q_{tot1} are free from the Knudsen-layer corrections.

The form of Eq. (B42) is the same in the Knudsen layer at the resting plate ($x_1 = d$). The corresponding corrections $\rho_K^{(1)}$ and $T_K^{(1)}$ are obtained by replacing (x_1, v_1) with $(d - x_1, -v_1)$, defining y by $y = \rho_B(d - x_1)/\epsilon$, and noting that the subscript B indicates the values at $x_1 = d$ in Eq. (B44).

APPENDIX C: DATA AND ACCURACY TEST FOR NUMERICAL COMPUTATION

First, we summarize the data for the numerical computation. We have used uniform cells in x_1 . The number of the cells N_x per length $d_0 = 2\pi\sqrt{5/6} = 5.7357\dots$ is common to all the results shown in the figures and is 2000 (note that $N = N_x$ for $d = d_0$, $N = 3N_x$ for $d = 3d_0$, etc.). Therefore, the size of a cell Δx when the oscillating plate is located at $x_1 = 0$ is $\Delta x = d_0/2000 = 0.0028\dots$. The time step is also uniform and the number of steps N_t per period is from 3.2×10^5 to 1.28×10^6 . More precisely, the time step is $\Delta t = 2\pi/3.2 \times 10^5 = 1.9\dots \times 10^{-5}$ for the result shown in Figs. 2, 3, 5, and 6; $\Delta t = 2\pi/6.4 \times 10^5 = 9.8\dots \times 10^{-6}$ for Fig. 4; and $\Delta t = 2\pi/1.28 \times 10^6 = 4.9\dots \times 10^{-6}$ for Fig. 7. The Δx and Δt for the results shown in Figs. 8, 9, and 11 are more or less based on the data given above.

We next give some examples of the accuracy check. Hereafter, we consider the case of $\epsilon = 0.1$, $a_w = 0.1$, and $d = d_0$. In the following, we use the four grid systems: grid 1, $\Delta x = d_0/500 = 1.1\dots \times 10^{-2}$ and $\Delta t = 2\pi/8 \times 10^4 = 7.8\dots \times 10^{-5}$; grid 2, $\Delta x = d_0/1000 = 5.7\dots \times 10^{-3}$ and $\Delta t = 2\pi/1.6 \times 10^5 = 3.9\dots \times 10^{-5}$; grid 3, $\Delta x = d_0/2000 = 2.8\dots \times 10^{-3}$ and $\Delta t = 2\pi/3.2 \times 10^5 = 1.9\dots \times 10^{-5}$; and grid 4, $\Delta x = d_0/4000 = 1.4\dots \times 10^{-3}$ and $\Delta t = 2\pi/6.4 \times 10^5 = 9.8\dots \times 10^{-6}$.

Let h stand for ρ , v_1 , T , and p and let h^{G_i} denote the result of h based on the grid (grid i) ($i = 1, 2, 3, 4$). At $t/2\pi = 200$, we have $|h^{G1} - h^{G4}| < 1.2 \times 10^{-4}$, $|h^{G2} - h^{G4}| < 3.3 \times 10^{-5}$, and $|h^{G3} - h^{G4}| < 8.6 \times 10^{-6}$. This shows that the grid systems used in the computation have given the results of sufficient accuracy. Here Δt and Δx are related as $\Delta t = c\Delta x$ with $c = 0.006846\dots$, so the scheme (48) should have second-order accuracy in x (see the last paragraph in Sec. VI A). The errors listed here are consistent with the second-order accuracy. Similar checks have been carried out by changing Δx for a fixed Δt ($\Delta t = 9.8\dots \times 10^{-6}$) and by changing Δt for a fixed Δx ($\Delta x = 1.1\dots \times 10^{-2}$), but the results are omitted here.

The total mass of the gas between the two plates per unit area of the plates is expressed as

$$m(t) = \int_{x_w(t)}^d \rho(t, x_1) dx_1, \quad (\text{C1})$$

which is theoretically constant. However, because of numerical errors, it changes slightly with time. If we plot $|m(t) - m(0)|/m(0)$ versus t , it increases almost linearly in t , oscillating with an amplitude that does not increase with t , after some tens of the periods. We evaluated the average amplitude r_m [i.e., the average of the maximum minus the minimum in each period ($n < t/2\pi \leq n + 1$; $n = 100, 101, \dots, 199$) over $100 \leq t/2\pi \leq 200$] and the average rate of increase s_m of

the maximum per one period (i.e., the maximum in $199 < t/2\pi \leq 200$ minus the maximum in $100 < t/2\pi \leq 101$ divided by 100). The result is as follows: $r_m \approx 3.2 \times 10^{-6}$ and $s_m \approx 3.7 \times 10^{-8}$ for grid 1, $r_m \approx 8.3 \times 10^{-7}$ and $s_m \approx 1.8 \times 10^{-8}$ for grid 2, $r_m \approx 2.7 \times 10^{-7}$ and $s_m \approx 9.0 \times 10^{-9}$ for grid 3, and $r_m \approx 1.6 \times 10^{-7}$ and $s_m \approx 4.5 \times 10^{-9}$ for grid 4. The results show that better mass conservation is attained with finer grid systems.

Finally, we consider the momentum and energy transfer. In the time-periodic state, $\overline{\mathcal{P}^L} = \overline{\mathcal{P}^R}$ and $\overline{\mathcal{E}^L} = \overline{\mathcal{E}^R}$ hold (cf. Sec. VII B). We check how accurately these relations are satisfied numerically. Let us set $\mathcal{P}_{\text{err}} = (\overline{\mathcal{P}^L} - \overline{\mathcal{P}^R})/a_w$ and $\mathcal{E}_{\text{err}} = (\overline{\mathcal{E}^L} - \overline{\mathcal{E}^R})/a_w$. Then $\mathcal{P}_{\text{err}} \approx 3.2 \times 10^{-6}$ and $\mathcal{E}_{\text{err}} \approx 2.5 \times 10^{-4}$ (grid 1), $\mathcal{P}_{\text{err}} \approx -3.5 \times 10^{-6}$ and $\mathcal{E}_{\text{err}} \approx 2.5 \times 10^{-4}$ (grid 2), $\mathcal{P}_{\text{err}} \approx -6.8 \times 10^{-6}$ and $\mathcal{E}_{\text{err}} \approx 2.5 \times 10^{-4}$ (grid 3), and $\mathcal{P}_{\text{err}} \approx -8.2 \times 10^{-6}$ and $\mathcal{E}_{\text{err}} \approx 2.5 \times 10^{-4}$ (grid 4). This shows that the grid refinement (grid 1 \rightarrow grid 4) does not improve the conservation properties of momentum and energy. On the other hand, we obtained a better result: $\mathcal{P}_{\text{err}} \approx 4.0 \times 10^{-7}$ and $\mathcal{E}_{\text{err}} \approx 3.2 \times 10^{-5}$ for the grid system with $\Delta x = d_0/500 = 1.1 \dots \times 10^{-2}$ and $\Delta t = 2\pi/6.4 \times 10^5 = 9.8 \dots \times 10^{-6}$. This and other tests suggest that to have better momentum and energy conservation, smaller time steps are required.

-
- [1] G. Russo and F. Filbet, Semilagrangian schemes applied to moving boundary problems for the BGK model of rarefied gas dynamics, *Kinet. Relat. Models* **2**, 231 (2009).
 - [2] S. Chen, K. Xu, C. Lee, and Q. Cai, A unified gas kinetic scheme with moving mesh and velocity space adaptation, *J. Comput. Phys.* **231**, 6643 (2012).
 - [3] M. Inaba, T. Yano, and M. Watanabe, Linear theory of sound waves with evaporation and condensation, *Fluid Dyn. Res.* **44**, 025506 (2012).
 - [4] T. Tsuji and K. Aoki, Moving boundary problems for a rarefied gas: Spatially one-dimensional case, *J. Comput. Phys.* **250**, 574 (2013).
 - [5] V. Kolobov, R. Arslanbekov, and A. Frolova, in *Proceedings of the 29th International Symposium on Rarefied Gas Dynamics 2014*, edited by J. Fan, AIP Conf. Proc. No. 1628 (AIP, Melville, 2014), pp. 952–961.
 - [6] G. Dechristé and L. Mieussens, A Cartesian cut cell method for rarefied flow simulations around moving obstacles, *J. Comput. Phys.* **314**, 465 (2016).
 - [7] Y. W. Yap and J. E. Sader, Sphere oscillating in a rarefied gas, *J. Fluid Mech.* **794**, 109 (2016).
 - [8] G. Karniadakis, A. Beskok, and N. Aluru, *Microflows and Nanoflows: Fundamentals and Simulation* (Springer, New York, 2005).
 - [9] S. Hutcherson and W. Ye, On the squeeze-film damping of micro-resonators in the free-molecule regime, *J. Micromech. Microeng.* **14**, 1726 (2004).
 - [10] M. Bao and H. Yang, Squeeze film air damping in MEMS, *Sensor. Actuator. A* **136**, 3 (2007).
 - [11] X. Guo and A. Alexeenko, Compact model of squeeze-film damping based on rarefied flow simulations, *J. Micromech. Microeng.* **19**, 045026 (2009).
 - [12] L. Desvillettes and S. Lorenzani, Sound wave resonances in micro-electro-mechanical systems devices vibrating at high frequencies according to the kinetic theory of gases, *Phys. Fluids* **24**, 092001 (2012).
 - [13] S. K. Loyalka and T. C. Cheng, Sound-wave propagation in a rarefied gas, *Phys. Fluids* **22**, 830 (1979).
 - [14] J. R. Thomas, Jr. and C. E. Siewert, Sound-wave propagation in a rarefied gas, *Transport Theory Stat. Phys.* **8**, 219 (1979).
 - [15] S. Stefanov, P. Gospodinov, and C. Cercignani, Monte Carlo simulation and Navier-Stokes finite difference calculation of unsteady-state rarefied gas flows, *Phys. Fluids* **10**, 289 (1998).
 - [16] T. Ohwada and M. Kunihisa, in *Rarefied Gas Dynamics*, edited by A. D. Ketsdever and E. P. Muntz (AIP, Melville, 2003), pp. 202–209.
 - [17] N. G. Hadjiconstantinou and A. L. Garcia, Molecular simulations of sound wave propagation in simple gases, *Phys. Fluids* **13**, 1040 (2001).

- [18] R. D. M. Garcia and C. E. Siewert, The linearized Boltzmann equation: Sound-wave propagation in a rarefied gas, *Z. Angew. Math. Phys.* **57**, 94 (2006).
- [19] D. Kalempa and F. Sharipov, Sound propagation through a rarefied gas confined between source and receptor at arbitrary Knudsen number and sound frequency, *Phys. Fluids* **21**, 103601 (2009).
- [20] T. Tsuji and K. Aoki, in *Proceedings of the 28th International Symposium on Rarefied Gas Dynamics 2012*, edited by M. Mareschal and A. Santos, AIP Conf. Proc. No. 1501 (AIP, Melville, 2012), pp. 115–122.
- [21] T. Tsuji and K. Aoki, Gas motion in a microgap between a stationary plate and a plate oscillating in its normal direction, *Microfluid. Nanofluid.* **16**, 1033 (2014).
- [22] C. Cercignani, *The Boltzmann Equation and Its Applications* (Springer, Berlin, 1988).
- [23] C. Cercignani, *Rarefied Gas Dynamics: From Basic Concepts to Actual Calculations* (Cambridge University Press, Cambridge, 2000).
- [24] Y. Sone, *Kinetic Theory and Fluid Dynamics* (Birkhäuser, Boston, 2002); Kyoto University research information repository, supplementary notes and errata, available at <http://hdl.handle.net/2433/66099>.
- [25] Y. Sone, *Molecular Gas Dynamics: Theory, Techniques, and Applications* (Birkhäuser, Boston, 2007); Kyoto University research information repository, supplementary notes and errata, available at <http://hdl.handle.net/2433/66098>.
- [26] P. L. Bhatnagar, E. P. Gross, and M. Krook, A model for collision processes in gases. I. Small amplitude processes in charged and neutral one-component systems, *Phys. Rev.* **94**, 511 (1954).
- [27] P. Welander, On the temperature jump in a rarefied gas, *Ark. Fys.* **7**, 507 (1954).
- [28] Y. Sone, in *Rarefied Gas Dynamics*, edited by L. Trilling and H. Y. Wachman (Academic, New York, 1969), pp. 243–253.
- [29] Y. Sone, in *Rarefied Gas Dynamics*, edited by D. Dini (Editrice Tecnico Scientifica, Pisa, 1971), Vol. II, pp. 737–749.
- [30] Y. Sone and K. Aoki, Steady gas flows past bodies at small Knudsen numbers—Boltzmann and hydrodynamic systems, *Transport Theory Stat. Phys.* **16**, 189 (1987).
- [31] Y. Sone, in *Advances in Kinetic Theory and Continuum Mechanics*, edited by R. Gatignol and Soubbaramayer (Springer, Berlin, 1991), pp. 19–31.
- [32] Y. Sone, K. Aoki, S. Takata, H. Sugimoto, and A. V. Bobylev, Inappropriateness of the heat-conduction equation for description of a temperature field of a stationary gas in the continuum limit: Examination by asymptotic analysis and numerical computation of the Boltzmann equation, *Phys. Fluids* **8**, 628 (1996).
- [33] Y. Sone, C. Bardos, F. Golse, and H. Sugimoto, Asymptotic theory of the Boltzmann system, for a steady flow of a slightly rarefied gas with a finite Mach number: General theory, *Eur. J. Mech. B* **19**, 325 (2000).
- [34] S. Takata and M. Hattori, Asymptotic theory for the time-dependent behavior of a slightly rarefied gas over a smooth solid boundary, *J. Stat. Phys.* **147**, 1182 (2012).
- [35] M. Hattori and S. Takata, Second-order Knudsen-layer analysis for the generalized slip-flow theory I, *Bull. Inst. Math. Acad. Sinica* **10**, 423 (2015).
- [36] M. Hattori and S. Takata, Second-order Knudsen-layer analysis for the generalized slip-flow theory II: Curvature effects, *J. Stat. Phys.* **161**, 1010 (2015).
- [37] F. Coron, Derivation of slip boundary conditions for the Navier-Stokes system from the Boltzmann equation, *J. Stat. Phys.* **54**, 829 (1989).
- [38] K. Aoki, R. Kagaya, S. Kosuge, and H. Yoshida, in *Proceedings of the 29th International Symposium on Rarefied Gas Dynamics 2014* (Ref. [5]), pp. 60–67.
- [39] H. Grad, in *Handbuch der Physik*, Band XII, edited by S. Flügge (Springer, Berlin, 1958), pp. 205–294.
- [40] S. Chapman and T. G. Cowling, *The Mathematical Theory of Non-uniform Gases*, 3rd ed. (Cambridge University Press, Cambridge, 1991).
- [41] H. Tang and T. Tang, Adaptive mesh methods for one- and two-dimensional hyperbolic conservation laws, *SIAM J. Numer. Anal.* **41**, 487 (2003).
- [42] H. Tang and T. Tang, Multi-dimensional moving mesh methods for shock computations, *Contemp. Math.* **330**, 169 (2003).
- [43] Y. Inoue and T. Yano, Propagation of strongly nonlinear plane waves, *J. Acoust. Soc. Am.* **94**, 1632 (1993).
- [44] T. Yano and Y. Inoue, Quasisteady streaming with rarefaction effect induced by asymmetric sawtooth-like plane waves, *Phys. Fluids* **8**, 2537 (1996).

- [45] C. L. Pekeris and Z. Alterman, Solution of the Boltzmann-Hilbert integral equation II. The coefficients of viscosity and heat conduction, *Proc. Natl. Acad. Sci. U.S.A.* **43**, 998 (1957).
- [46] T. Ohwada and Y. Sone, Analysis of thermal stress slip flow and negative thermophoresis using the Boltzmann equation for hard-sphere molecules, *Eur. J. Mech. B* **11**, 389 (1992).
- [47] H. Grad, in *Transport Theory*, edited by R. Bellman, G. Birkhoff, and I. Abu-Shumays (American Mathematical Society, Providence, 1969), pp. 269–308.
- [48] C. Bardos, R. E. Caflisch, and B. Nicolaenko, The Milne and Kramers problems for the Boltzmann equation of a hard sphere gas, *Commun. Pure Appl. Math.* **39**, 323 (1986).
- [49] F. Coron, F. Golse, and C. Sulem, A classification of well-posed kinetic layer problems, *Commun. Pure Appl. Math.* **41**, 409 (1988).
- [50] F. Golse, Analysis of the boundary layer equation in the kinetic theory of gases, *Bull. Inst. Math. Acad. Sinica* **3**, 211 (2008).
- [51] Y. Sone, Effect of sudden change of wall temperature in rarefied gas, *J. Phys. Soc. Jpn.* **20**, 222 (1965).
- [52] S. K. Loyalka and J. H. Ferziger, Model dependence of temperature slip coefficient, *Phys. Fluids* **11**, 1668 (1968).
- [53] C. E. Siewert and J. R. Thomas, Jr., Half-space problems in the kinetic theory of gases, *Phys. Fluids* **16**, 1557 (1973).
- [54] Y. Sone, T. Ohwada, and K. Aoki, Temperature jump and Knudsen layer in a rarefied gas over a plane wall: Numerical analysis of the linearized Boltzmann equation for hard-sphere molecules, *Phys. Fluids A* **1**, 363 (1989).
- [55] Y. Sone and Y. Onishi, Kinetic theory of evaporation and condensation, *J. Phys. Soc. Jpn.* **35**, 1773 (1973).
- [56] Y. Sone and Y. Onishi, Kinetic theory of evaporation and condensation: Hydrodynamic equation and slip boundary condition, *J. Phys. Soc. Jpn.* **44**, 1981 (1978).